International Geology Review

ISSN: 0020-6814 (Print) 1938-2839 (Online) Journal homepage: www.tandfonline.com/journals/tigr20

# Geochemistry, U-Pb and Sm-Nd isotopic constraints on Rhyacian metamafic-metaultramafic plutonic rocks in the southern São Francisco paleocontinent, Mineiro belt, Brazil: petrogenesis and tectonic implications

Marco Aurélio Piacentini Pinheiro, Ciro Alexandre Ávila, Joana Reis Magalhães, Catarina Labouré Benfica Toledo, Márcio Antônio Silva, Everton Marques Bongiolo, Francisco Teixeira Vilela, Mahyra Tedeschi, George Luiz Luvizotto & Wilson Teixeira

**To cite this article:** Marco Aurélio Piacentini Pinheiro, Ciro Alexandre Ávila, Joana Reis Magalhães, Catarina Labouré Benfica Toledo, Márcio Antônio Silva, Everton Marques Bongiolo, Francisco Teixeira Vilela, Mahyra Tedeschi, George Luiz Luvizotto & Wilson Teixeira (08 Feb 2026): Geochemistry, U-Pb and Sm-Nd isotopic constraints on Rhyacian metamafic-metaultramafic plutonic rocks in the southern São Francisco paleocontinent, Mineiro belt, Brazil: petrogenesis and tectonic implications, International Geology Review, DOI: 10.1080/00206814.2026.2623123

**To link to this article:** https://doi.org/10.1080/00206814.2026.2623123

INTERNATIONAL GEOLOGY REVIEW
https://doi.org/10.1080/00206814.2026.2623123

Taylor & Francis
Taylor & Francis Group



# Geochemistry, U-Pb and Sm-Nd isotopic constraints on Rhyacian metamafic-metaultramafic plutonic rocks in the southern São Francisco paleocontinent, Mineiro belt, Brazil: petrogenesis and tectonic implications

Marco Aurélio Piacentini Pinheiro[a], Ciro Alexandre Ávila[b], Joana Reis Magalhães[c], Catarina Labouré Benfica Toledo[d], Márcio Antônio Silva[c], Everton Marques Bongiolo[e], Francisco Teixeira Vilela[c], Mahyra Tedeschi[f], George Luiz Luvizotto[g] and Wilson Teixeira[h]

[a]Geological Survey of Brazil, Center of Applied Geosciences – CGA, CPRM/SGB, Rio de Janeiro, Brazil; [b]Programa de Pós-Graduação Patrimônio Geopaleontológico, Museu Nacional, Universidade Federal do Rio de Janeiro, Rio de Janeiro, Brazil; [c]Geological Survey of Brazil, Directory of Geology and Mineral Resources – CPRM/SGB, Belo Horizonte, Brazil; [d]Instituto de Geociências, Universidade de Brasília, Brasília, Brazil; [e]Programa de Pós-GraduaçãoemGeociências, Universidade Federal do Rio Grande do Sul, UFRGS, Porto Alegre, Brazil; [f]Geological Survey of Finland, Espoo, Finland; [g]Instituto de Geociências e Ciências Exatas, Universidade Estadual Paulista, UNESP, Rio Claro, Brazil; [h]Instituto de Geociências, Universidade de São Paulo, USP, São Paulo, Brazil

**ABSTRACT**

Mafic and ultramafic rocks are crucial for understanding the Earth's evolution, offering insights into ancient crustal formation, orogenic processes, and continental assembly. This study examines the petrogenesis and metamorphic history of the Mineiro belt, a key Paleoproterozoic accretionary system in Brazil's southern São Francisco-Congo Paleocontinent. Using petrographic analysis, whole-rock and mineral geochemistry, and U-Pb and Sm-Nd isotopic data, we investigated the Rio Grande metagabbro, Forro metapyroxenites, and metaperidotites. Our findings reveal Rhyacian tholeiitic magmatism, with U-Pb zircon crystallization ages of 2111 ± 10 Ma and 2113 ± 14 Ma for the Rio Grande metagabbro and 2116 ± 39 Ma for the Forro metapyroxenite. These ages correlate with the fifth Paleoproterozoic mafic-ultramafic magmatism episode (2.18–2.10 Ga) in the SFCP and Columbia supercontinent formation. Isotopic signatures indicate a depleted mantle source with minor crustal contamination (εNd(t) = -0.46 to +4.10) and Neoarchean source influence (2.72–2.78 Ga TDM ages). Metamorphic evolution includes early greenschist facies hydration, followed by amphibolite facies metamorphism and a later low-grade overprint. Furthermore, we identified a Neoproterozoic anatectic event (590 Ma) that affected the Rio Grande metagabbro, constraining a period of crustal reworking associated with the Western Gondwana assembly and inward decratonisation along the southern São Francisco craton margins.

**ARTICLE HISTORY**
Received 16 June 2025
Accepted 8 November 2025

**KEYWORDS**
Mafic-ultramafic plutonic rocks; Rhyacian crystallization; paleoproterozoic metamorphism; neoproterozoic anatexis; melt patches domains; Columbia supercontinent

## 1. Introduction

The Archaean-Paleoproterozoic transition is characterized by several global changes, including the Great Oxidation Event (GOE) and the diversification of geological environments, including the transition from tonalite-trondhjemite-granodiorite (TTGs) assemblages to basalt-andesite-dacite-rhyolite (BADR) associations, a worldwide decrease in komatiite occurrences, and a consequent decline in the formation of volcanic ultramafic melts (Guo *et al*. 2009; Condie 2015; Gaucher and Frei 2018; Liebmann *et al*. 2021). In this context, mafic and ultramafic rocks and their associated crustal units play a key role in the investigation of Earth's evolution over time. They serve as essential tools in the reconstruction and distribution of ancient crustal blocks, deciphering the evolution of accretionary orogens and the processes of continental assembly (Green and Ringwood 1969; Pearce and Cann 1973; Sun and McDonough 1989; Pearce 2008, 2014; Condie 2015; Profeta *et al*. 2016).

In particular, the interval between 2.45–2.20 Ga marks a widespread reduction in the frequency of both detrital and igneous zircon U-Pb ages, alongside a decrease in magmatic activity and the formation of granitoids. This period was initially designated as the 'Magmatic shutdown' (Condie and Aster 2009) or 'Tectono-Magmatic Lull' (Spencer *et al*. 2018). Recently, Condie *et al*. (2022) revisited this subject and reduced this interval to 2.36–2.23 Ga, during which the rate of orogenic activity and global magma production decreased.

On a supercontinental scale, several palaeogeographic reconstructions have been proposed for this period,

**CONTACT** Marco Aurélio Piacentini Pinheiro marcopiacentini@gmail.com Geological Survey of Brazil, Center of Applied Geosciences – CGA, CPRM/SGB, 404 Pasteur Avenue Urca, Rio de Janeiro, RJ 22290-240, Brazil
Supplemental data for this article can be accessed online at https://doi.org/10.1080/00206814.2026.2623123.

based on geodynamic, tectonic, and isotopic-palaeomagnetic evidence (Liebmann *et al*. 2021; D'Agrella-Filho *et al*. 2022). Despite some agreement with the connection of numerous crustal blocks during 2.1–1.8 Ga, the role of the São Francisco-Congo Paleocontinent (SFCP) within these models remains an open question. Certain reconstructions suggest that this paleocontinent was linked to the Columbia supercontinent; however, there is no consensus on its internal configuration or the arrangement of its crustal blocks (Rogers and Santosh 2002; Zhao *et al*. 2004; Hou *et al*. 2008; Cederberg *et al*. 2016; D'Agrella-Filho and Cordani 2017; Chaves 2021; Meert and Santosh 2022). Alternative models have also been proposed, considering the SFCP outside Columbia (e.g. D'Agrella-Filho and Cordani 2017). Despite significant research on Paleoproterozoic palaeogeography, the role of the São Francisco-Congo Paleocontinent (SFCP) remains a key unknown.

This study provides new geological and isotopic evidence from specific metamafic and metaultramafic rocks, offering insights into the SFCP's evolution and its place in ancient continental reconstructions. In this study, we provide new evidence of petrography, whole rock and mineral chemistry, zircon U-Pb SHRIMP ages, and Sm-Nd isotope data from metamafic and metaultramafic samples of the Rio Grande metagabbro and the Forro-layered metaperidotite-metapyroxenite, which are key units of the Mineiro belt, and on the role of the SFCP. These rocks are contemporaneous with the evolution of the main Paleoproterozoic accretionary period of the southern SFCP (Teixeira *et al*. 2015; Barbosa and Barbosa 2017; Heilbron *et al*. 2017; Barbosa *et al*. 2019; Pinheiro *et al*. 2022).

We also report the first Ediacaran U-Pb zircon crystallization ages in the Mineiro belt. These ages are associated with melt-patch zones situated along localized high-strain domains and coincide with the main period of the Western Gondwana assembly along the southern São Francisco craton (SFC). The new data provide valuable geodynamic proxies for reconstructing Paleoproterozoic terranes in the southern SFCP and offer insights into the composition and reconstruction of the Columbia and Gondwana supercontinents.

## 2. Geological setting

The SFC (Figure 1(A)) represents one of the ancient nuclei of the South American platform and records a long geodynamic evolution that started in the Paleoarchean (3.6–3.5 Ga) in its northern part (Silva *et al*. 2016; Barbosa *et al*. 2020; Oliveira *et al*. 2020) and in the Palaeo to Mesoarchean (3.26–3.20 Ga) in its southern part (Lana *et al*. 2013; Simon *et al*. 2021). The SFC, together with its African counterpart (the Congo craton), constitutes the SFCP, a landmass composed of Archaean nuclei and Paleoproterozoic magmatic arcs, which were amalgamated during the Siderian-Orosirian orogenic processes associated with the Minas-Bahia orogeny (Bruno *et al*. 2021).

Main lithodemic units from Mineiro belt (modified from Cardoso *et al*. 2019). Age references in Supplementary Table S1 and the sample coordinates are in Supplementary Table S3.

### 2.1. The Mineiro belt

The Mineiro belt, located in the southern SFC (Figure 1), is bounded by two major lineaments: Jeceaba-Bom Sucesso and Congonhas-Itaverava (Figure 2). The first lineament separates the north-northwest domains of the Mineiro belt from the Archaean polycyclic crust. The Congonhas-Itaverava lineament is at the northeastern limit of the Mineiro belt, bounding the Archaean rocks collectively known as part of the Quadrilátero Ferrífero (Seixas *et al*. 2012, 2013; Moreira *et al*. 2018). The southern and southwestern limits of the Mineiro belt are associated with two distinct thrust systems that juxtapose Neoproterozoic sequences and Archaean-Paleoproterozoic shortened crust as part of the assembly of Western Gondwana (Campos Neto and Caby 2000; Alkmim *et al*. 2001; Trouw *et al*. 2013; Marimon *et al*. 2023), as well as the Piedade Block, an Archaean microcontinent with ages between 2731 ± 34 and 2523 ± 28 Ma (Bruno *et al*. 2021).

Despite the major faults that bound the Mineiro belt, several internal lineaments played a significant role in its internal framework. The most prominent is the Lenheiro Shear Zone LSZ (Figure 2), which divides the Mineiro belt into northern and southern blocks composed of distinct geologic units (Ávila *et al*. 2010, 2014; Teixeira *et al*. 2022).

The northern block (Figure 2; Supplementary Table S1) comprises three main units: (i) 2.47–2.31 Ga arc-type tonalitic-trondhjemitic orthogneisses, including the Cassiterita, Lagoa Dourada, Ramos and Resende Costa plutons (Seixas *et al*. 2012; Teixeira *et al*. 2015; Barbosa *et al*. 2019); (ii) 2.25–2.20 Ga metavolcano-sedimentary sequences (Ávila *et al*. 2010; Teixeira *et al*. 2015, 2022); and (iii) 2.19–2.00 Ga orthogneisses, metadiorites and metagranitoides (Barbosa *et al*. 2015; Cardoso *et al*. 2019; Neves *et al*. 2023; Sousa *et al*. 2023; Lacerda *et al*. 2024), together with coeval sanukitoides (Moreira *et al*. 2020).

The southern block hosts distinct groups of Rhyacian rocks (Figure 2): (i) 2.23–2.20 Ga metasubvolcanic and metavolcanic calc-alkaline rocks of Serrinha and

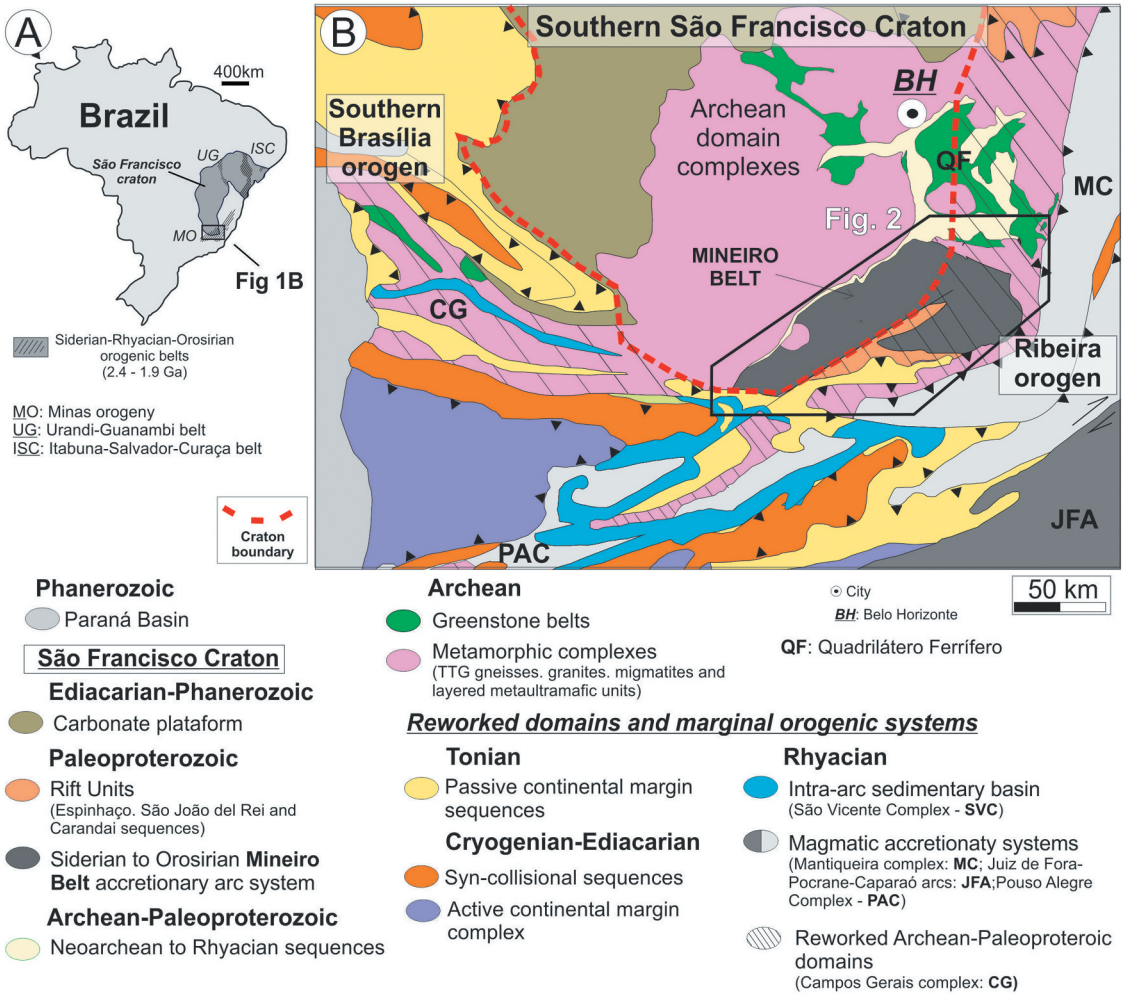


**Figure 1.** Geological map of the southern São Francisco craton (modified from Silva *et al*. 2016; Pinheiro *et al*. 2019). (A) Position of the São Francisco craton on Brazil and their main Siderian-Orosirian orogenic systems. (B) Simplified geology of the southern São Francisco craton. The Mineiro belt is detailed in Figure 2.

Tiradentes suites (Ávila et al. 2010, 2014); (ii) 2.24–2.22 Ga komatiite-bearing metavolcanic-sedimentary sequences, namely the Nazareno and Dores de Campos units (Ávila *et al*. 2014); (iii) 2.22–2.18 Ga metagabbroid rocks (Valença *et al*. 2000; Vieira 2015); (iv) 2.19–2.15 Ga high-K and calc-alkaline orthogneisses, and 2.14–2.08 Ga calc-alkaline metagranitoides, as the Represa de Camargos and Gentio plutons (Barbosa *et al*. 2015; Neves *et al*. 2023; Silva *et al*. 2021); and (v) Estação Tiradentes metasedimentary sequence, which is younger than 2.04 Ga (Ávila *et al*. 2014–Figure 2 and Supplementary Table S1).

### 2.2. Paleoproterozoic mafic and ultramafic rocks in the Mineiro belt

Mafic and ultramafic rocks are common components of the Paleoproterozoic crust of the Mineiro belt, and their generation is recognized along seven distinct time-related groups (Table 1). The ages of these rocks fit within the main interval of orthogneisses, tonalites, and granite crystallization related to four magmatic arcs. The early event may have been associated with Archaean metabasalts or amphibolites that underwent melting at ca. 2.5–2.4 Ga to produce the protolith of the Cassiterita orthogneiss, as suggested by Sm-Nd $T_{DM}$ ages (Barbosa *et al*. 2019). A similar scenario is also envisaged for the generation of the mafic protolith of the TTG-signatured orthogneisses from the 2.35–2.31 Ga Resende Costa, Ramos and Lagoa Dourada plutons, as their $T_{DM}$ ages fall between 2.5–2.4 Ga (Seixas *et al*. 2012; Teixeira *et al*. 2015). A second basic magma generation is correlated with the protolith crystallization of the 2.32 Ga Restinga de Cima amphibolite, with $T_{DM}$ ages of 2.4 and 2.7 Ga (Teixeira *et al*. 2015). These two generations of mafic and ultramafic rocks correlate with the interval between the Cassiterita and Resende Costa arcs.

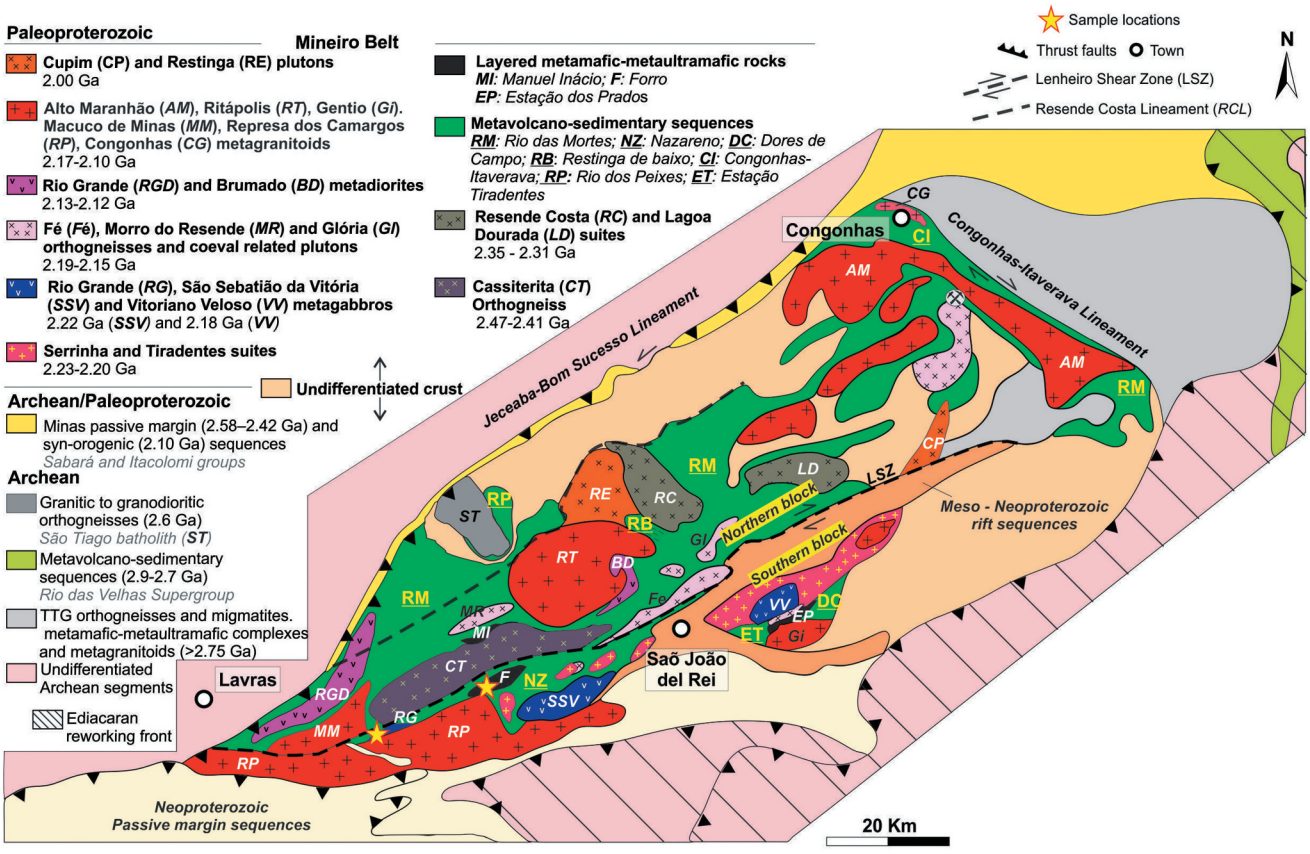


**Figure 2.** Main lithodemic units from Mineiro belt (modified from Cardoso *et al*. 2019). Age references in Supplementary table S1 and the sample coordinates are in Supplementary table S3.

The third generation corresponds to metakomatiites and amphibolites (high-Mg and tholeiitic basalts) associated with the Nazareno and Dores de Campos metavolcano-sedimentary sequences. The amphibolites from these units yielded crystallization ages of 2.26–2.22 Ga (Ávila *et al*. 2014). The fourth generation is associated with the intrusion of the São Sebastião da Vitória (2.22 Ga; Valença *et al*. 2000) and Vitoriano Veloso (2.18 Ga; Vieira 2015) metagabbros over the Nazareno and Dores de Campos metavolcano-sedimentary sequences. The third and fourth mafic and ultramafic rock formations correlate with the evolution of the Serrinha arc.

The fifth generation of basic magmas ranges in age from 2.18 to 2.10 Ga. It includes amphibolite outcropping in the Quadrilátero Ferrífero area and dismembered mafic-ultramafic rocks in the southernmost Brasilia orogen (Table 1). The Rio Grande metagabbro and the Forro-layered metaperidotite-metapyroxenite fit into this interval, which is correlated with the evolution of the Ritápolis arc (Barbosa *et al*. 2015; Alkmim and Teixeira 2017).

The sixth generation of basic magmas is associated with dikes/sills in the eastern cratonic inlier, with ages between 2.04–1.99 Ga (Bruno *et al*. 2020; Carvalho *et al*. 2024), in addition to the Paraopeba dike swarm in the Quadrilátero Ferrífero, with ages between 2.02–1.92 Ga (Mendes *et al*. 2022). The final Paleoproterozoic mafic rocks are associated with intracontinental bimodal magmatism of Statherian age (~1.79–1.71 Ga), documented in the southern and western portions of the SFC. This magmatism is related to the opening of a slip-related rift system (Magalhães *et al*. 2018) and coeval mafic dyke swarms (Cederberg *et al*. 2016; Caxito *et al*. 2020; Chaves 2021). The sixth interval corresponds to the late stage of orogenic development of the Mineiro belt, while the final interval aligns with the rift phase, occurring late in orogenic collapse.

## 3. Methods

The methods applied in this work include geological mapping (1:50.000), petrography, representative mineral chemistry of samples, whole-rock lithochemistry, isotopic Sm-Nd analysis, and (SHRIMP) zircon U-Th-Pb geochronology of three representative samples. The supplementary material presents all

**Table 1.** Metamafic and metaultramafic rocks of Paleoproterozoic age in the southern São Francisco craton and related marginal domains. References: 1: Teixeira *et al.* (2015); 2: Ávila *et al.* (2014); 3: Valença *et al.* (2000); 4: Vieira (2015); 5: this work; 6: Cabral *et al.* (2022); 7: Cabral and Zeh (2015); 8: Pinheiro *et al.* (2019); 9: Westin *et al.* (2016); 10: Pinheiro *et al.* (2022); 11: Mendes *et al.* (2022); 12: Bruno *et al.* (2020); 13: Magalhães *et al.* (2018); 14: Caxito *et al.* (2020); 15: Cederberg *et al.* (2016). Crystallization age method: *LA-ICP-MS (in zircon grains); **SHRIMP (in zircon grains); **tt: SHRIMP (in titanite grains); **bd: SHRIMP (in baddeleyite grains); # inferred from the field relationship. MB: mineiro belt; SSFC: southern São Francisco craton; QF: quadrilátero Ferrífero province; MC: mantiqueira complex; SBO: southern Brasilia orogen; CGD: Campos Gerais domain; GD: guanhães domain.

| Mafic- ultramafic magamtism | Rock Type | Geological association | Geotectonic unit interpretation | Domain | Locallity | Cristallyzation age | Metamorphic age | TDM (Ga) | eNd(t) | eHf(t) | Sample | Ref |
|---|---|---|---|---|---|---|---|---|---|---|---|---|
| 1 | Metabasalts | Restinga de Baixo amphibolite (Archaean metabasalts) | Cassiterita arc | MB | Cassiterita; northern Mineiro belt | >2.47 Ga # | – | – | – | – | – | 1 |
| 2 | Amphibolites (metabasalts) | Restinga de Cima amphibolite | Resende Costa arc | | Resende Costa; northern Mineiro belt | 2318 ± 16 Ma* | – | 2.5–2.7 | +4 to +8 | – | FG-14 | |
| 3 | Komatiites and high-Mg basalts | Volcano-sedimentary sequence | Plateou or oceanic-type lithosphere | | Northern and southern Mineiro belt | 2255 ± 51 and 2223 ± 4 Ma* | – | | | | - | 2 |
| 4 | Metagabbro | São Sebastião da Vitória metagabbro | Serrinha arc | | São Sebastião da Vitória; southern Mineiro belt | 2220 ± 3 Ma* | – | 2.2 | – | – | – | 3 |
| | Metadiabase | Vitoriano Veloso metagabbro | Serrinha arc | | Vitoriano Veloso; southern Mineiro belt | 2183 ± 11 Ma** | – | | - | – | TH-06 | 4 |
| | Metagabbro | | | | | 2193 ± 12 Ma** | – | 2.2 | – | – | JU-000 | |
| | | | | | | 2175 ± 32 Ma (**tt) | – | 2.3 | – | – | JU-000 | |
| 5 | Amphibolites | Rio Grande metagabbro | Intraoceanic-type lithosphere | | Nazareno; southern Mineiro belt | 2135 ± 33 Ma** | 596 ± 4 Ma | | - | – | FV99 | 5 |
| | Metagabbro | | | | | 2130 ± 33 Ma** | 587 ± 3 Ma | | - | – | FV100 | |
| | Metapyroxenite | Forro layered rocks | | | | 2116 ± 39 Ma** | – | | - | – | FV167 | |
| | Indurated crust (canga-like plateau) | Possible metabasalt (pillow lava) | Minas basin related volcanism | SSFC and QF | Western low strain domain of QF | 2141 ± 6 Ma* | – | – | – | – | RM08 | 6 |
| | Soft material (canga-like plateau) | | | | | | – | – | – | – | RM09 | |
| | Amphibolite | Flows or sills of basaltic rock | | | Sítio Largo, eastern QF | 2155 ± 22 Ma* | 499 ± 23 Ma | – | – | – | SL1 | 7 |
| | Amphibolite | | | | | 2188 ± 24 Ma* | 495 ± 19 Ma | – | – | – | SL2 | |

(*Continued*)

**Table 1.** (Continued).

| Mafic- ultramafic magamtism | Rock Type | Geological association | Geotectonic unit interpretation | Domain | Locallity | Cristallyzation age | Metamorphic age | TDM (Ga) | eNd(t) | eHf(t) | Sample | Ref |
|---|---|---|---|---|---|---|---|---|---|---|---|---|
| | Spl-ol-opx granofels | Differentiated ultramafic rocks | São Vicente Complex; intraoceanic basin | SBO | Córrego da Areia; Carrancas Klippe | 2101 ± 6 Ma** | 573 ± 40 Ma | – | – | – | S280 | 8 |
| | Amphibolite | Metabasalts | | | São Vicente de Minas; Andrelandia Nappe System | 2143 ± 9 Ma** | – | – | 3.52 | – | S264 | |
| | Amphibolite | | | | Andrelândia; Andrelandia Nappe System | 2144 ± 9 Ma** | 597 ± 23 Ma | – | – | – | S271A | |
| | Amphibolite | | | | Andrelândia; Andrelandia Nappe System | 2145 ± 9 Ma** | – | – | 4.26 | – | And6 | |
| | Amphibolite | | | | Ibitipoca; Andrelandia Nappe System | 2146 ± 9 Ma** | – | – | 3.48 | – | Ibit01 | |
| | Amphibolite | | | | Ibitipoca; Andrelandia Nappe System | 2118 ± 59 Ma** | – | – | 2.67 | – | Ibit02 | |
| | Amphibolite | | | | Ibitipoca; Andrelandia Nappe System | 2136 ± 17 Ma* | 681 ± 170 Ma | 2.2 | 3.4 | +5.8 to +8.2 | C509 | 9 |
| | Amphibolite | | | | Carrancas; Carrancas Klippe | 2143 ± 14 Ma* | 568 ± 14 Ma | 2.4 | 3.5 | – | C540 | |
| | Ol-opx granofels | Differentiated ultramafic rocks | | CGD | Nova Resende; Petúnia Complex | 2132 ± 7 Ma** | 659 ± 2 Ma | – | – | – | Pet015 | 10 |
| 6 | Amphibolite | Dikes of basaltic rock | Paraopeba dike swarms | SSFC and QF | Pau branco; QF | 2019 ± 23 Ma* | – | – | – | −20.8 to 29.0 | PB | 11 |
| | Amphibolite | | | | Várzea dos Lopes; QF | 1944 ± 29 Ma* | 595 ± 65 Ma | – | – | −30.6 to 33.1 | VL | |
| | Amphibolite | | | | Casa de Pedra; QF | 1918 ± 12 Ma* | – | – | – | −23.7 to 10.3 | CP | |
| | Amphibolite | Dikes or sills of basaltic rock | | MC | Abre Campo | 2044 ± 6 Ma* | 661 ± 64 Ma | – | – | – | 103C | 12 |
| | Amphibolite | | | | | 1989 ± 13 Ma* | 610 ± 33 Ma | – | – | – | 70D | |
| 7 | Metabasalt (amphibolite) | Intraplate basalts (SLIP) and rift-related dike swarms | Alto Rio Guanhães unit | GD | Guanhães domain | 1725 ± 4 Ma* | – | 2.28 to 2.44 | – | −8.25 to −4.05 | J02 | 13 |
| | Dolerite | | Pará de Minas dike swarms | SSFC | Divinópolis Complex | 1799 ± 37 Ma**bd | – | 3 | −10.04 | – | P6 | 14 |
| | Porphyritic dolerite | | | | Divinópolis Complex | 1736 ± 63 Ma**bd | – | 2.9 | −8.92 | – | P1 | |
| | Dolerite | | | | Campo Belo Complex | 1716 ± 53 Ma**bd | – | – | – | – | P8 | |
| | Dolerite | | | | Campo Belo Complex | 1798 ± 4 Ma**bd | – | – | – | – | MG-3 | 15 |
| | Dolerite | | | | Divinópolis Complex | 1702 ± 13 Ma**bd | – | – | – | – | MG-4 | |
| | Dolerite | | | | Campo Belo Complex | 1791 ± 7 Ma**bd | – | – | – | – | MG-5 | |
| | Dolerite | | | | Campo Belo Complex | 1793 ± 18 Ma**bd | – | – | – | – | MG-6 | |
| | Porphyritic dolerite | | | | Campo Belo Complex | 1717 ± 11 Ma**bd | – | – | – | – | MG-7 | |

methods used here and their related materials and techniques.

## 4. Results

### 4.1. Local geology

The Rio Grande metagabbro is an E-W striking body extending over 500 m, located in the southern block of the Mineiro belt and hosted by metakomatiites and metabasalts of the 2.26–2.22 Ga Nazareno metavolcano-sedimentary sequence (Figure 2). The metagabbro is coarse-grained and shows an isotropic variety with localized metric-scale compositional layering (Figure 3(A)). Locally, it grades into a metamelanogabbro and metapyroxenite. The primary magmatic structures were locally overprinted by deformations along their margins. Internal, fine-grained amphibolites and mylonitic-ultramylonitic rocks are also present, associated with submeter-scale high-strain zones (Figure 3(B,C)). Intrusive metagranitoids of ca. 2086 ± 12 Ma (Barbosa *et al*. 2015) constrain its minimum age (Figure 3(D)).

The Forro-layered metaperidotite-metapyroxenite is an E-W striking massif composed of course- to medium-grained serpentinized metaperidotites and metapyroxenites. It occurs in the southern block of the Mineiro belt and is associated with the same metavolcano-sedimentary sequence as the Rio Grande metagabbro (Figure 2). Along the shear zones, talc-tremolite-chlorite-serpentine schists, serpentinites, and mylonites occur mainly as lithotypes (Figure 4(A,B)).

#### 4.1.1. Rio Grande metagabbro

The main lithotype of the Rio Grande metagabbro body is coarse-grained (1–6 mm) metagabbro with subophitic to intergranular textures. Despite the preserved igneous features, no primary minerals were identified. Its lithotypes are composed of Ca-amphibole aggregates (pseudomorphs after clinopyroxene) surrounded by a groundmass of recrystallized plagioclase, which is associated with fine-grained epidote, zoisite, clinozoisite, and subordinate sericite (Figure 5(A,B)). Accessory minerals include titanite, ilmenite, quartz, chalcopyrite, zircon, and apatite.

Deformation in the metagabbro-imprinted foliation to high-strain mylonites (Figure 5(C,D)). Ca-amphibole varies from actinolite to hornblende and occurs in four main ways: (i) pseudomorphic grains (2–6 mm) after primary clinopyroxene (Figure 5(A,B)) with actinolite cores grading to hornblende rims (Figure 5(C-E)); (ii) stretched and oriented grains parallel to the main foliation (Figure 5(C,D)), associated with amphibolites and mylonites in high-strain zones; (iii) fine-grained hypidioblastic to idioblastic neocrystals overgrowing the matrix and hornblende crystals (Figure 5(A)); and (iv) idioblastic neocrystals after peritectic diopside (Figure 5(F)). The

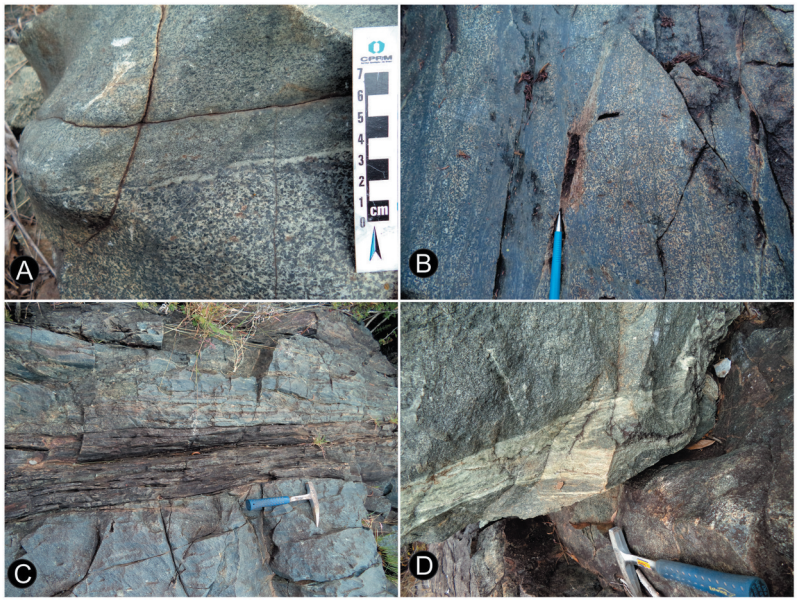


**Figure 3.** Macroscopic features of the Rio Grande metagabbro. (A) Distinct mineralogical and textural facies of the metagabbro protolith. Coarse-grained facies with sub-ophitic texture grading to equigranular medium-grained facies with felsic layer in the contact. Presence of Ca-amphibole and plagioclase in the coarse-grained facies. (B) Coarse-grained facies with Ca-amphibole and plagioclase (light domains) partially overprinted by irregular recrystallization lamellae and zones of fine-grained amphibolites (dark domains). (C) Sub-metric shear zone in the metagabbro, forming mylonitic and ultramylonitic rocks. (D) Early Rhyacian granitic dike crosscutting the metagabbro.

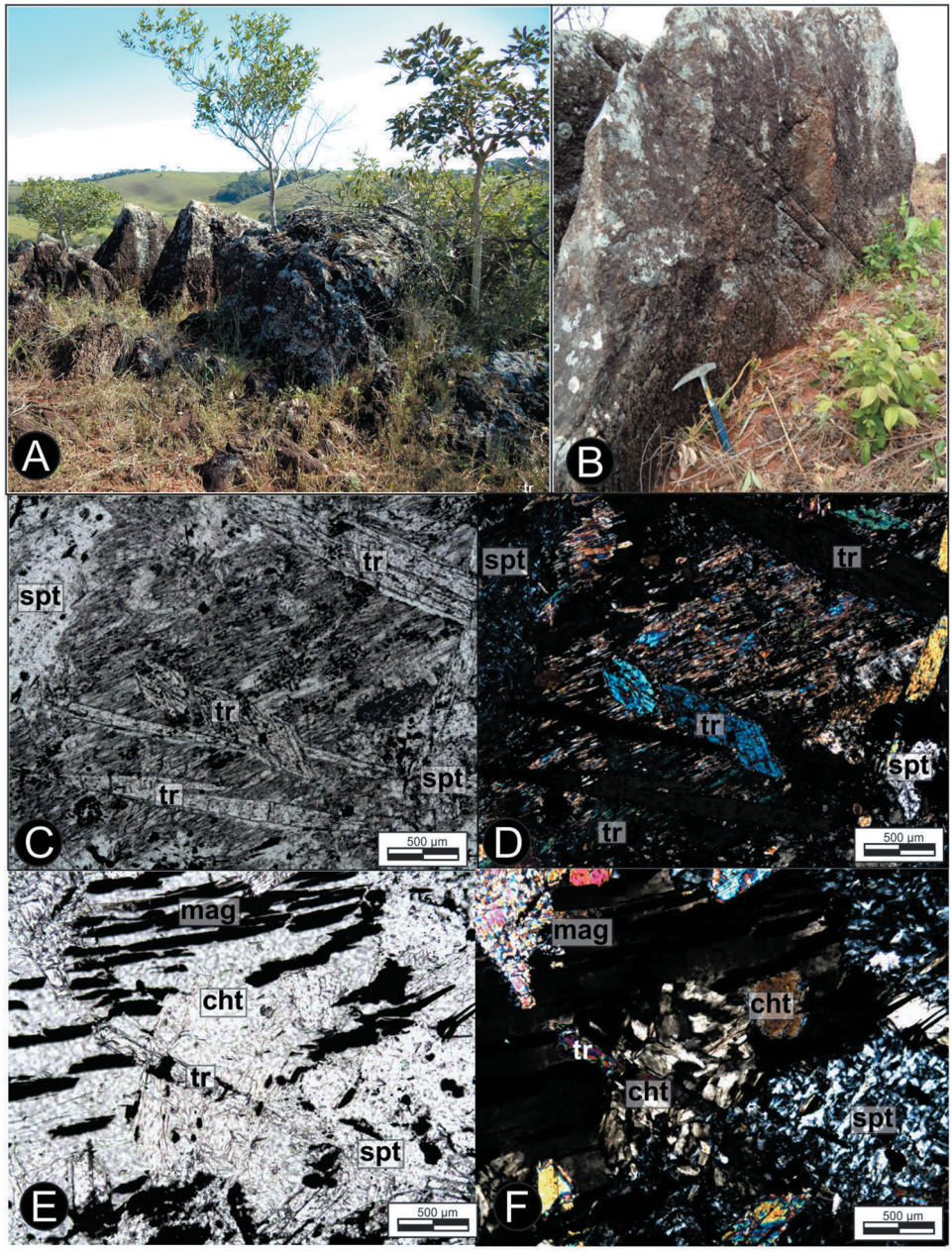


**Figure 4.** Macroscopic and petrographic features of serpentinites of the Forro layered metaperidotite-metapyroxenites. (A) Outcrop of serpentinite (after pyroxenite). (B) Detail of textural layering in metaperidotite. (C) and (D) Late tremolite (tr) that overgrowths serpentine (spt) rich groundmass (parallel and crossed polarized light). (E) and (F) Pseudomorph aggregates of chlorite (cht) and serpentine (spt) after primary cumulus phases, as olivine and pyroxene, with late magnetite (mag) and tremolite (tr) overgrowths (parallel and crossed polarized light).

plagioclase grains are hypidiomorphic, interstitial, and medium-to coarse-grained (1–3 mm). They were highly recrystallized and moderately replaced by epidote, zoisite, clinozoisite, and sericite (Figure 5(A,B)). Ilmenite occurs as fine- to medium-grained xenoblastic grains, preferentially oriented along the main foliation, and rimmed by titanite.

The Rio Grande metagabbro shows localized features of partial melting along the high-strain zones, represented by melt-patch domains (Figure 6(A,B)). These domains were further categorized into three subdomains. The first is characterized by irregular, coarse-grained ( >2 cm) peritectic diopside aggregates ( > 90%) (Figure 6(B,C)), defining melanocratic domains (melanosomes) with subordinate small aggregates of interstitial plagioclase (and quartz) along grain boundaries and cleavage surfaces. The second subdomain is irregular, discordant, and hololeucocratic (neossome or

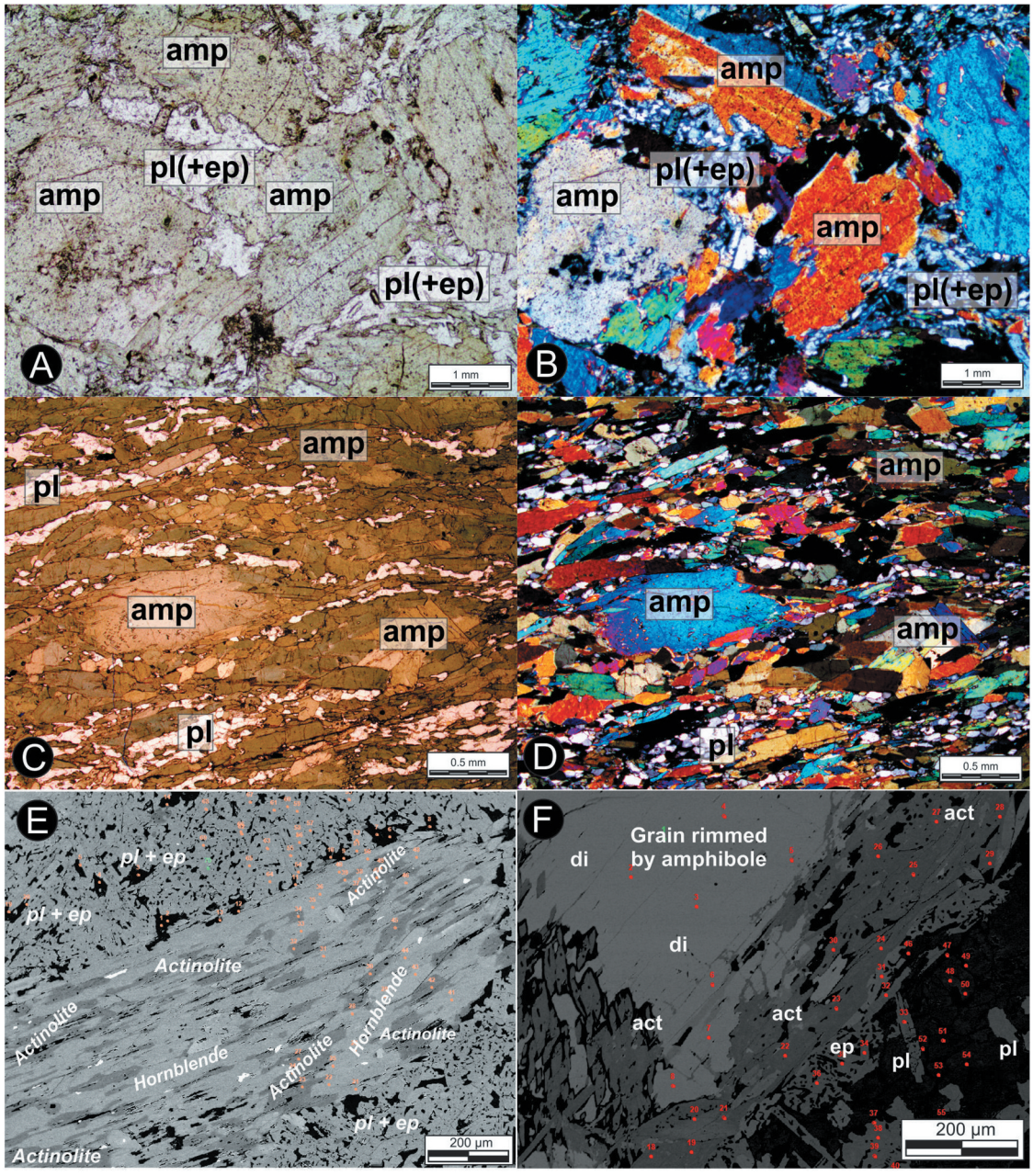


**Figure 5.** Petrographic features of the Rio Grande metagabbro. (A and B) Pseudomorphic texture with Ca-amphibole crystals (amp) and secondary plagioclase with fine-grained epidote, zoisite, clinozoisite and sericite (pl + ep) replacement in parallel and crossed polarized light. (C and D) Amphibolite with nematoblastic-texture showing Ca-amphibole (amp) and recrystallized plagioclase (pl + ep) orientated along the main foliation at higher strain sites in parallel and crossed polarized light. (E) Backscattered image showing an amphibole grain with early actinolite partially recrystallized to magnesium-hornblende. (F) Backscattered image showing late actinolite (act) alteration (uralitization), associated with plagioclase (pl) and epidote (ep), overgrowing inward peritectic clinopyroxene with a diopside (di) composition. The red dots indicate the locations of the mineral chemistry analyses.

plagioclasite) and is composed of up to 95% undeformed and twinned plagioclase and minor epidote grains (Figure 6(C)). It is straight-edged and characterized by flow-oriented grains and 120° dihedral triple junctions of plagioclase, typical of fine-grained annealed igneous rocks. Finally, the last subdomain was represented by fine- to medium-grained amphibolites and mylonites composed of stretched amphibole, recrystallized plagioclase, and minor epidote (Figure 6(C)). It is interpreted as the paleosome of the localized anatectic system, occurring as an envelope around the first and second domains, and is itself enclosed by plagioclasite (neosome) (Figure 6 (B,C)).

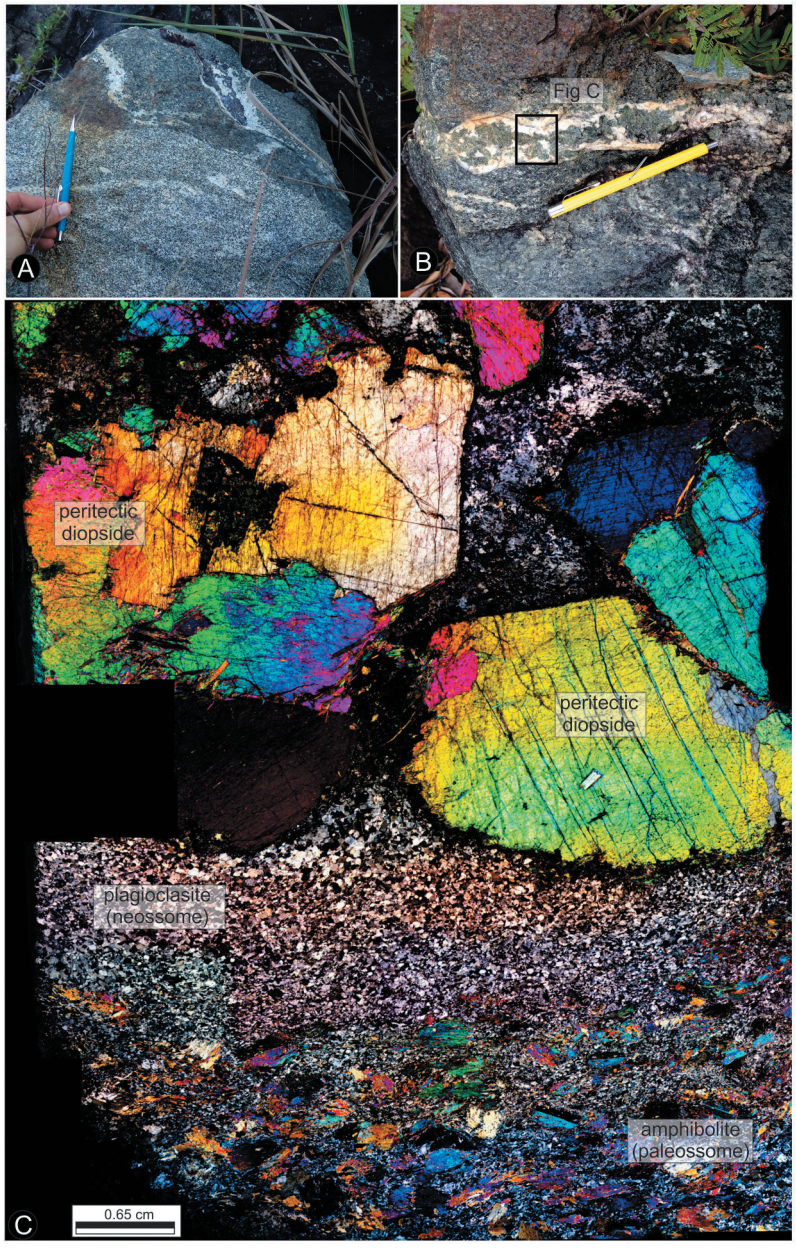


**Figure 6.** Field and petrographic features of the melt patch domains in the Rio Grande metagabro. (A) Fine-grained felsic melt patch domain discordant to the main foliation. (B) Detail of the melt patch domain with coarse-grained diopside (light green) involved by an aggregate of fine-grained plagioclase and epidote (white). (C) Photomosaic in parallel and crossed polarized light of melt patch domains subdivided in three subdomains: (i) melanocratic layer rich in coarse-grained peritectic diopside (melanossome) and fine-grained plagioclase and epidote in the upper portion of the image; (ii) hololeucocratic layer rich (neossome) in the center represented by fine-grained plagioclase and epidote, named plagioclasite; and (iii) mesocratic layer rich in fine-grained and orientated amphibole and plagioclase crystals (amphibolite – paleossome) in the lower portion of the image. The protolith of this domain is gabbroic rocks of the Rio Grande metagabbro (see text to further explanations).

Within the metagabbro, remnant patches of actinolite appear irregular and enclosed within highly pseudomorphosed magnesium-hornblende grains. These grains were surrounded by a recrystallized groundmass composed of oligoclase and epidote (clinozoisite). Actinolite in the melt patch domain has two forms: recrystallized pseudomorphic grains that occasionally contain rare remnants of a magnesium-hornblende core (Figure 5(E)) and uralitized rims surrounding diopside peritectic grains (Figure 5(F)). The inclusions of actinolite within the coarse-grained peritectic diopside highlight the presence of a Ca-amphibole phase in the early mineral assemblage preceding the diopside formation (Figure 6(F)).

#### 4.1.2. Forro layered metaperidotite-metapyroxenite

The metaperidotites from the Forro-layered metaperidotite-metapyroxenite exhibit metre-scale tabular primary igneous layers defined by variations in both the composition and texture (Figure 4(A,B)). These layers are mainly composed of serpentine, chlorite, tremolite, cummingtonite, and magnesium-hornblende, with the most common modal distribution showing a predominance of serpentine ( > 50%). These minerals comprise a variety of amphibole-chlorite serpentinites and chlorite-amphibole-serpentine schists. Anthophyllite, talc, magnetite, and ilmenite are minor phases, whereas chalcopyrite and pentlandite are accessory minerals.

Although their primary mineral assemblages were absent, certain igneous features remained preserved. Poikilitic mesocumulate textures are characterized by coarse-grained hypidioblastic tremolite, chlorite, and serpentine pseudomorphs after orthopyroxene and olivine cumulus grains. These pseudomorphs are enclosed by post-cumulus clinopyroxene oikocrysts (8–11 mm) that have been entirely replaced by zoned amphibole grains with opaque-rich tremolite cores and inclusion-free cummingtonite rims. Serpentine is associated with two distinct hydration episodes: an early stage involving primary olivine, and a second stage involving residual olivine, Ca-amphiboles, and chlorite. Early hydration resulted in coarse-grained pseudomorphs of felty-textured serpentine aggregates. Subsequently, the textural relationship is characterized by the recrystallization of lepidoblastic serpentine and chlorite and the onset of nematoblastic amphibole (Figure 4(C,D)), resulting in serpentinite, tremolite, and chlorite-bearing schists and mylonites.

Tremolite and anthophyllite occur as fine- to medium-grained tabular to acicular grains, ranging from idioblastic to xenoblastic. Chlorite also reflects two stages of hydration: one after primary minerals such as orthopyroxene and olivine, and another after amphibole and serpentine (along with earlier chlorite) during a later event. Magnetite is xenoblastic, fine-grained, recrystallized along the main foliation, and is included in amphiboles.

The metapyroxenites are medium- to coarse-grained rocks primarily composed of chlorite, amphibole, and serpentine, with minor amounts of magnetite, ilmenite, accessory pyrite, chalcopyrite, and apatite. Despite the absence of primary minerals, the early textures were preserved as equigranular phases surrounded by oikocrysts, indicating meso- to accumulate textures (Figure 4 (E,F)). The igneous phases, including olivine, orthopyroxene, and clinopyroxene, were entirely replaced. Equigranular pseudomorphs (approximately 0.5 mm) of serpentine aggregates replaced olivine, whereas idioblastic to subidioblastic (1.5–3.0 mm) pseudomorphs of chlorite and cummingtonite replaced early orthopyroxene. Evidence for clinopyroxene is based on inequigranular subhedral pseudomorphs (2–6 mm) of amphibole, with tremolite cores surrounded by cummingtonite. The post-cumulus phase is dominated by coarse-grained (4–8 mm) Ca-amphibole aggregates that replace poikilitic clinopyroxene (heteradcumulates). These aggregates exhibited tremolitic core domains enclosing fine-grained opaque minerals and inclusion-free cummingtonite rims. Magnetite occurs as fine-grained, recrystallized grains distributed along fractures and cleavages within amphibole and is closely associated with the onset of chlorite (Figure 4(E,F)). The serpentinites are composed of a serpentine-rich groundmass and opaque minerals with variable and minor amounts of amphibole, chlorite, and talc. The schists and mylonites define a diverse group of nematoblastic-textured rocks composed of chlorite and talc, which are found mainly at the margins and internal shear zones.

### 4.2. Mineral chemistry from the Rio Grande metagabbro

Mineral chemical analyses were performed on plagioclase, clinopyroxene, amphibole, and epidote in samples from the Rio Grande Metagabbro. The data are presented in Supplementary Table S2.

#### 4.2.1. Plagioclase

Plagioclase from the amphibolites occurs as fine-grained recrystallized aggregates (up to 50 µm). They present a compositional zoning defined by cores of oligoclase ($Ab_{70.9}An_{29.1}$-$Ab_{74.4}An_{25.6}$) rimmed by albite ($Ab_{93.6}An_{6.4}$ -$Ab_{96.4}An_{3.6}$) (Figure 7(A)) and partially recrystallized with actinolite and epidote (Figure 7(B-D)).

In the hololeucocratic portions of the melt patch domains, plagioclase defines granular aggregates with undeformed twinned magmatic features and inverse-pattern zoned grains. Andesine-labradorite cores ($Ab_{29.3}An_{70.7}$-$Ab_{57.4}An_{42.6}$) grade to labradorite and labradorite-bytownite ($An_{65–70}$) compositions at the rims (Figure 7(D-E)). Late albite outer zones occur close to epidote-rich domains (Figure 7(C)).

#### 4.2.2. Clinopyroxene

Clinopyroxene is restricted to melt patch domains and occurs unzoned, anhedral, coarse-grained, and contains actinolite inclusions. It has a diopside composition ($Di_{49–52}En_{23–39}Fs_{10–15}$- Figure 8(A)), with low $Al_2O_3$ (0.17–0.94 wt%) and $TiO_2$ (up to 0.42 wt%). Chemical modifications occur in grains with intense to moderate uralitization, with the development of actinolite at their

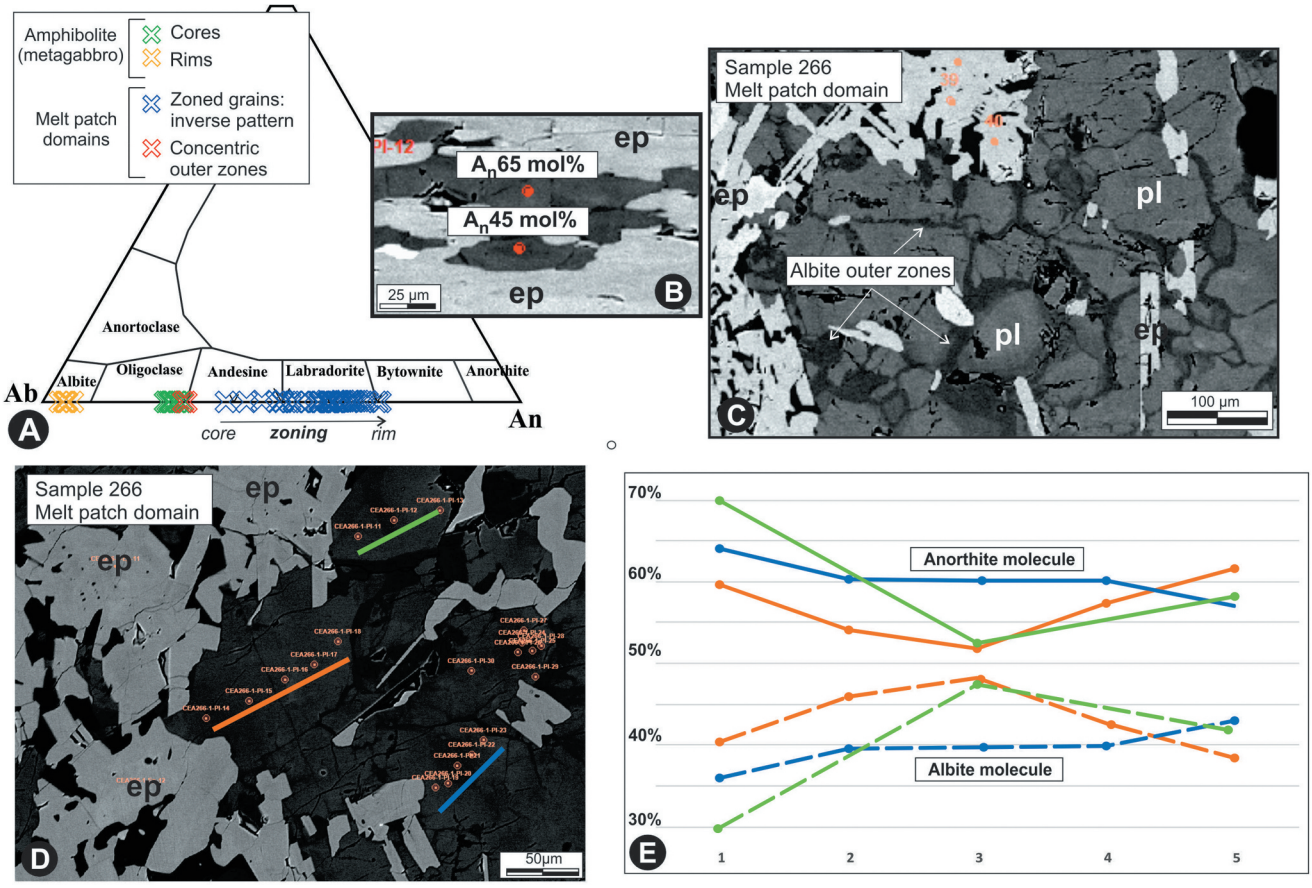


**Figure 7.** Mineral chemistry of plagioclase from amphibolite (metagabbro) samples and those from melt patch domains. (A) Ternary diagram of feldspar classification. (B) Backscattered image showing inverse compositional zoning of plagioclase, with anorthite-poor cores surrounded by anorthite-rich concentric domains. Epidote (Ep) around. (C) Backscattered image showing albite outer zones in plagioclase (pl) aggregates from melt patch domains. Epidote (Ep) around. (D and E) Chemical profile and the corresponding profile plot along plagioclase grains from melt patch domains.

edges. Coarse grains and grains rimmed by amphibole showed positive correlations between MgO and $SiO_2$ (Figure 8(B)). The profiles along coarse grains showed that some domains exhibited an inverse correlation between MgO and FeO (Figure 8(C)). In addition, these grains are depleted in $SiO_2$ and $Al^{VI}$ and enriched in $Al^{IV}$ compared to amphibole-rimmed grains (Figure 8(D-E)).

### 4.2.3. Amphibole

Chemical analyses were performed on amphibole grains from the metagabbros, amphibolites, and melt patch domains, including inclusions within peritectic clinopyroxene. The amphibole grains fall into two main compositional groups: actinolite and magnesium-hornblende (Figure 8(F)). In high-strain sites, the amphibole varies from magnesium hornblende in the cores to magnesium hornblende (with major TSi) and actinolite in the outer rims (Figure 8(F)).

Actinolite grains, associated with melt patch domains and metagabbros, have higher MgO and CaO contents than magnesium-hornblende grains (Figure 8(G)). Actinolite inclusions within peritectic clinopyroxene exhibited consistent CaO concentrations across the analysed grains, although their values were lower than those in the melt patch domains and metagabbro. The magnesium hornblende in metagabbro displays a homogeneous MgO content, while its CaO values vary subtly. In contrast, magnesium hornblende within the melt-patch domains showed greater compositional variability in both MgO and CaO (Figure 8(G)).

The relationship between the $Al^{IV}$ and $Al^{VI}$ cations in the amphibole structure follows a consistent linear trend in the metagabbro, melt patch domain, and clinopyroxene inclusions (Figure 8(H)). However, in the amphibolites and mylonites, the trend for these elements shows a clear separation from the other groups (Figure 8(H)).

### 4.2.4. Epidote

The epidote group minerals from the metagabbro and melt-patch domains exhibit a wide range of chemical

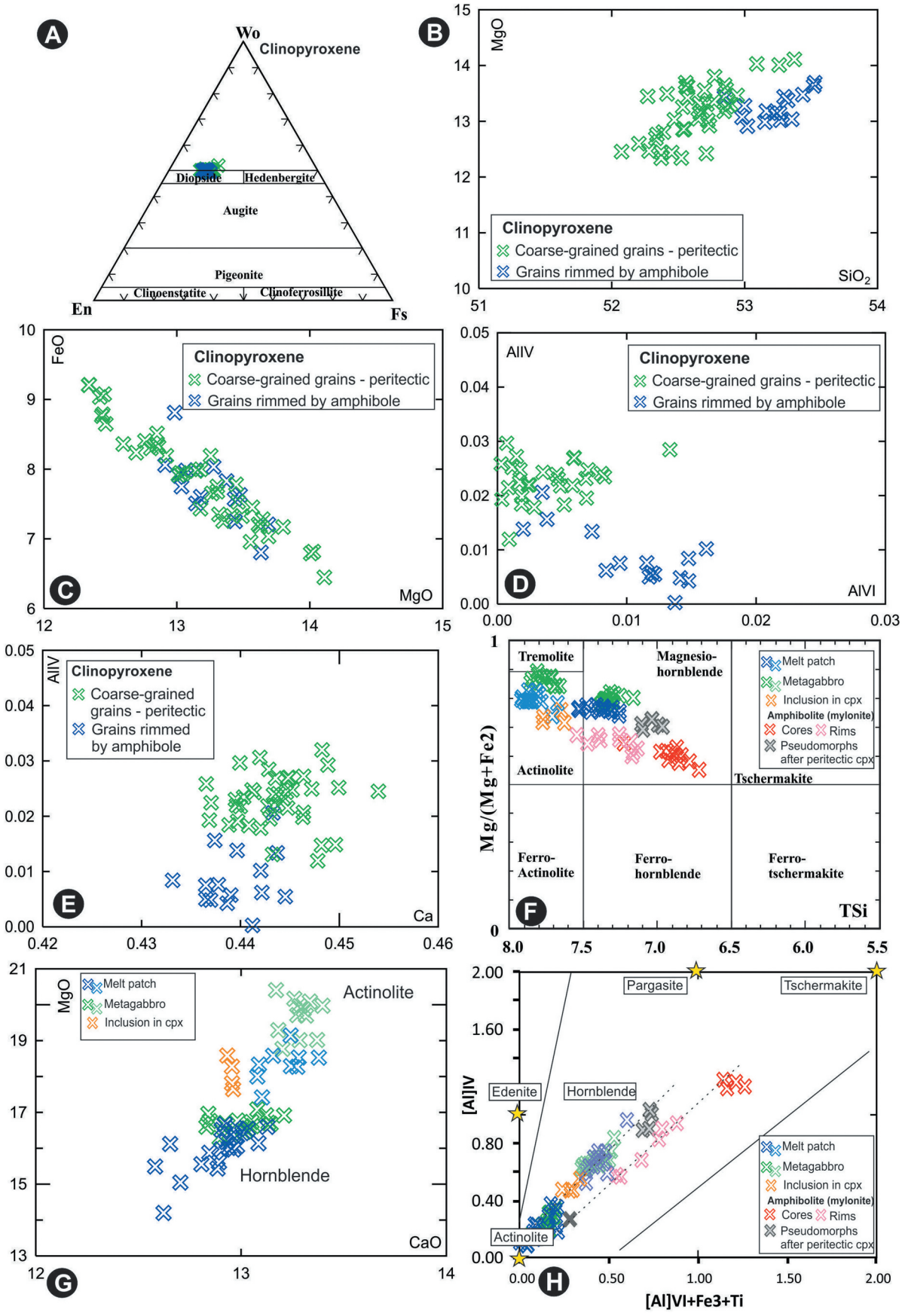


**Figure 8.** Diagrams for clinopyroxene and amphibole. (A) Ternary diagram of clinopyroxene classification (Morimoto *et al.* 1988) showing diopside composition. (B-E) Binary diagrams of clinopyroxone. (B) MgO (wt%) x SiO2 (wt%). (C) FeO (wt%) x MgO (wt%). (D) AlIV (apfu) ×AlVI (apfu). (E) AlIV (apfu) ×Ca (apfu) on the a site. (F) Mg/Mg+Fe + 2 ×TSi of amphibole classification (Hawthorne *et al.* 2012). (G) MgO (wt%) x CaO (wt%) with amphibole grains from the Rio Grande metagabbro, the melt patch domains and the diopside inclusions. H) AlIV (apfu) ×AlVI+Fe + 3+Ti + 4 (apfu) with two different trends.

compositions. Although both sets are composed of clinozoisite, the iron content varies considerably, ranging between 0.4–4.0 wt% ($Fe^{3+}$: 0.03–0.26 *apfu*) with CaO of 24.4–25.3 wt% (Ca: 12.00–12.90 *apfu*) and $Al_2O_3$ of 30.20–33.20 ($Al^{IV}$: 0.00–0.04 *apfu* and $Al^{VI}$: 2.70–2.90 *apfu*).

Although indistinguishable in terms of Ca and Si contents, grains from the melt patch domain near the peritectic clinopyroxene show a striking inverse relationship between Al and $Fe^{3+}$ (Figure in Supplementary Table S2). These grains have the highest $Fe_2O_3$ values recorded (above 1.3 wt% and up to 4.0 wt%), but the lowest Al content ( < 32.3 wt% $Al_2O_3$).

## 5. Whole-rock geochemistry

Whole rock chemical analyses were performed on twenty-eight samples, including nine from the Rio Grande metagabbro and 19 from the Forro-layered metaperidotite-metapyroxenite. These data are presented in Supplementary Table S3.

Rio Grande metagabbros, along with amphibolites and mylonites, display a range of compositions (Figure 9(A-E)): $SiO_2$ (47.8–51.7 wt%), MgO (5.7–13.0 wt %), $Fe_2O_3$t (4.7–15.5 wt%), $Al_2O_3$ (11.0–22.4 wt%), CaO (9.3–16.1 wt%), and Ti (110–304 ppm). The Cr and Ni contents vary between 1–400 ppm and 12–185 ppm, respectively. The LOI content ranges from 0.6–2.0 wt%.

The metaperidotites from the Forro layered metaperidotite-metapyroxenite have MgO contents between 28.7–38.9 wt%, $Fe_2O_3$t between 9.5–14.2 wt%, and $SiO_2$ between 45.5–49.1 wt%. The $Al_2O_3$ and CaO values are between 2.5–5.0 wt% and 1.5–7.3 wt%, respectively. Ni ranges from 1025 to 1925 ppm, Cr from 1960 to 3800 ppm, and Ti from 840 to 2880 ppm. LOI values vary from 4.2 to 10.0%. The metapyroxenites have higher $SiO_2$ (50.2–55.7 wt%) and lower MgO (20.5–30.0 wt%), along with CaO (1.5–2.2 wt%) and Ti (1080–2100 ppm). Although $Fe_2O_3$t values are slightly higher (11.0–12.1 wt%), $Al_2O_3$ (2.0–5.3 wt%), Cr (600–3800 ppm) and Ni (400–1420 ppm) remain similar. LOI values vary from 1.6–4.2 wt% (Figure 9(A-E)).

Samples from the Forro-layered metaperidotite – metapyroxenite and the Rio Grande metagabbro plot in tholeiitic and subalkaline fields in ternary diagrams (Figure 9(A,B)). Metaperidotites (and serpentinites) had higher MgO and LOI contents than the metagabros and amphibolites because of the presence of serpentine and chlorite in the former (Figure 9(C)). Despite post-magmatic alteration, MgO is strongly correlated with $SiO_2$ and Ni in binary diagrams normalized to $Al_2O_3$ (Figure 9(A-E)), suggesting some degree of element immobility and a preserved primary signature.

The trace and minor elements normalized to the Primitive Mantle (PM) delineate a slightly negative curve from Cs to Ce (LILE), marked by negative Nb and positive Rb and Pb anomalies. The HFSE pattern shows a slightly negative curve, ranging from near PM abundances to enrichments of up to 10 times its values, while remaining relatively flat from Pr to Lu (Figure 9(F)). REE delineated a slightly enriched negative to flat curve from La to Lu (Figure 9(G)).

## 6. U-Pb SHRIMP geochronology

Three samples were collected for zircon U-Pb SHRIMP geochronology: amphibolite (FV-99) and metagabbro (FV-100) from the Rio Grande metagabbro, and metapyroxenite from the Forro-layered metaperidotite-metapyroxenite (FV-167). The results are presented in Supplementary Table S4.

### *6.1. Amphibolite sample (FV-99)*

The amphibolite sample (FV-99) had zircon grains that could be grouped into three main populations. The predominant population is mainly subhedral, prismatic to pyramidal, with oscillatory zoning, 120–220 µm in length, and ratios of 2:1 to 3:1 (grains 2, 3, 6, 7, 8, 10, 11; Figure 10 (A)). In general, they show dark (grains 6, 10, and 11) or highly luminescent (grains 2, 3, and 8) individualized domains. The latter exhibited internal zoning truncated by irregular portions marked by engulfment. Some zircon cores appeared metamict, whereas others exhibited high U luminescence. Euhedral to subhedral grains characterized the second population with pyramidal terminations, lengths between 100–150 µm and ratios of 3:1 to 4:1. These crystals show oscillatory or parallel zoning with high luminescence bordered by new zircon growth that has low luminescence and is sometimes blurred (grains 4, 5, and 9; Figure 10(A)). Finally, the third population showed anhedral grains with rounded edges, lengths between 150–200 µm and a 3:1 ratio. These grains may have xenocrystic cores with different textures, such as sectorial or irregular zoning, overgrowth by oscillatory zoning, and resorption features (e.g. grains 1, 12, and 13; Figure 10(A)). All populations had overgrowth rims (~5 µm thick) with high to low luminescence.

Of the 15 spots in 13 grains analysed, eleven of which have a discordance of up to 5% and were predominantly dispersed along the Concordia. The rest of the grains showed a discordance between 9% and 39%. Five

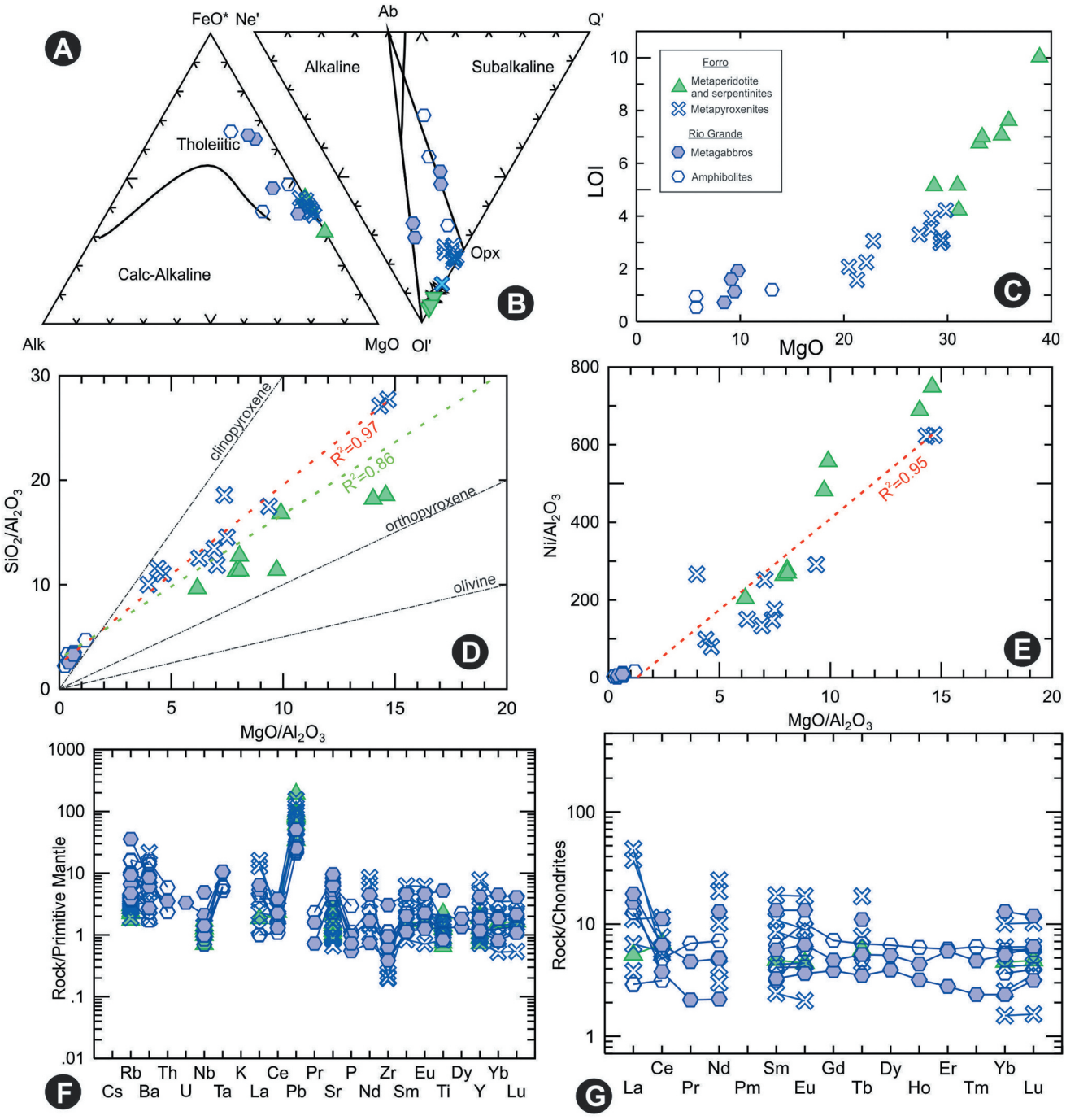


**Figure 9.** Plots of metaultramafic rocks (metaperidotites, metapyroxenites and serpentinites) from the Forro layered metaperidotite-metapyroxenites and metamafic rocks (metagabbros and amphibolites) from the Rio Grande metagabbro. (A and B) Ternary diagrams MgO-FeO*-alk (Na2O + K2O) and nefeline (ne) - quartz (Q) - olivine (ol) from Irvine and Baragar (1971). Ab = albite and opx = ortopyroxene. (C-E) Binary diagrams. C) LOI (wt%) x MgO (wt%). (D) SiO2 (wt%)/Al2O3 (wt%) x MgO (wt%)/Al2O3 (wt%). (E) Ni (ppm)/Al2O3 (wt%) x MgO (wt%)/Al2O3 (wt%). (F) Spider diagram with trace and minor elements normalized to primitive mantle (PM) of Sun and McDonough (1989). (G) Rare Earth elements (REE) normalized to chondrite of Sun and McDonough (1989). PM (REE) was not analysed.

analyses of the oscillatory zoning domains of four zircon grains of the first population yielded an upper intercept age of 2113 ± 14 Ma with an MSWD of 2.4 (Figure 11(A)), which was interpreted as the crystallization age of the amphibolite protolith. Three grains (2, 3, and 8) revealed Rhyacian inherited ages varying between 2161 ± 8 Ma and 2257 ± 11 Ma. One medium-dark core yielded an inherited age of 2746 ± 8 Ma (grain 7; Figure 11(A)).

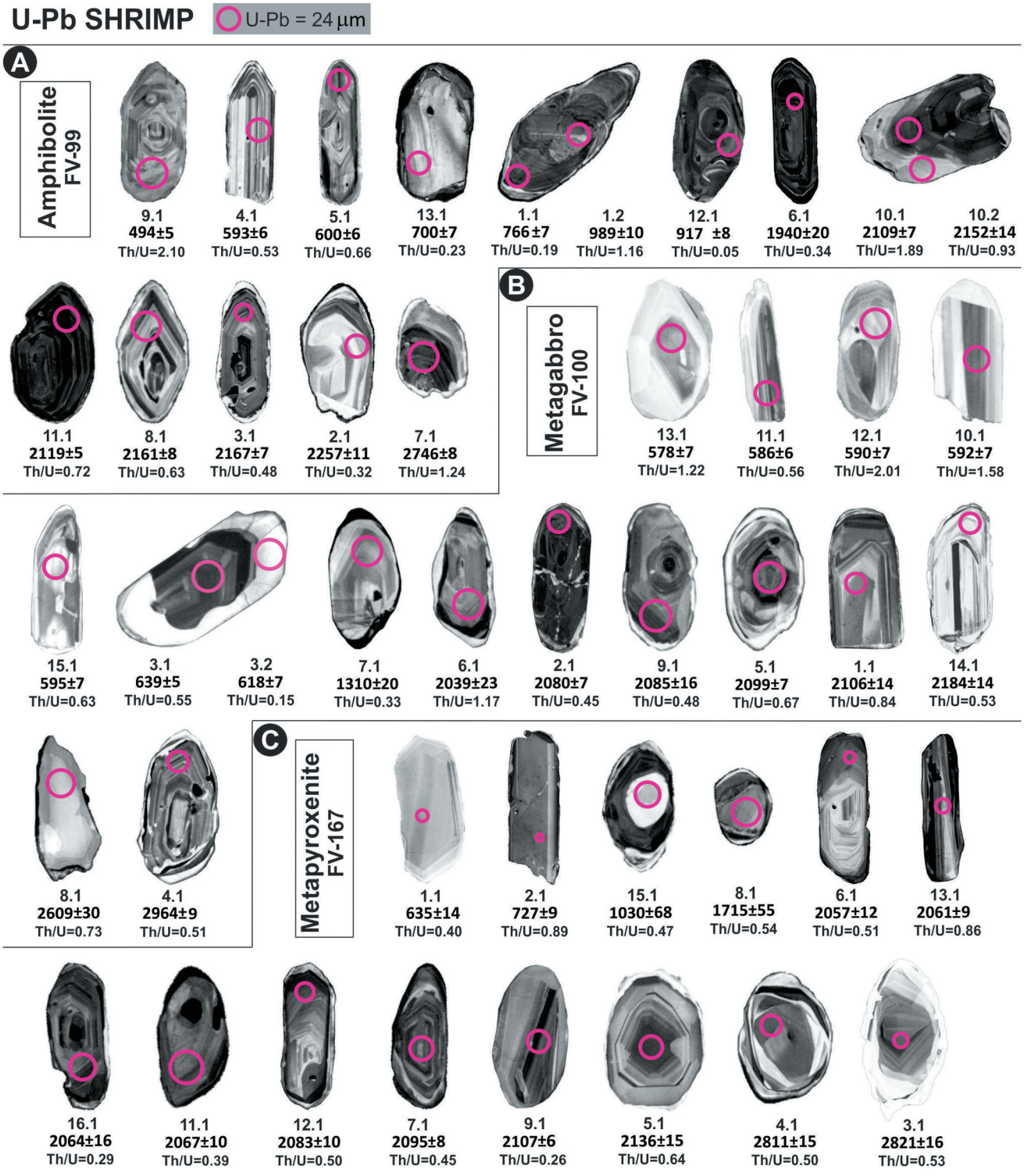


**Figure 10.** Cathodoluminescense images of analysed zircon grains from Rio Grande metagabbro and Forro layered metaperidotite-metapyroxenites. (A) Amphibolite (FV-99 - deformed gabbroic rock) from the Rio Grande metagabbro. (B) Metagabbro (FV-100) from the Rio Grande metagabbro. (C) Metapyroxenite (FV-167) from the Forro layered metaperidotite-metapyroxenites.

Moreover, two concordant analyses of the second population (grains 4 and 5) yielded an Ediacaran concordant age of 596 ± 4 Ma (Figure 11(B)). These grains show oscillatory zoning spots, suggesting igneous features related to the described anatectic system (melt patch domains).

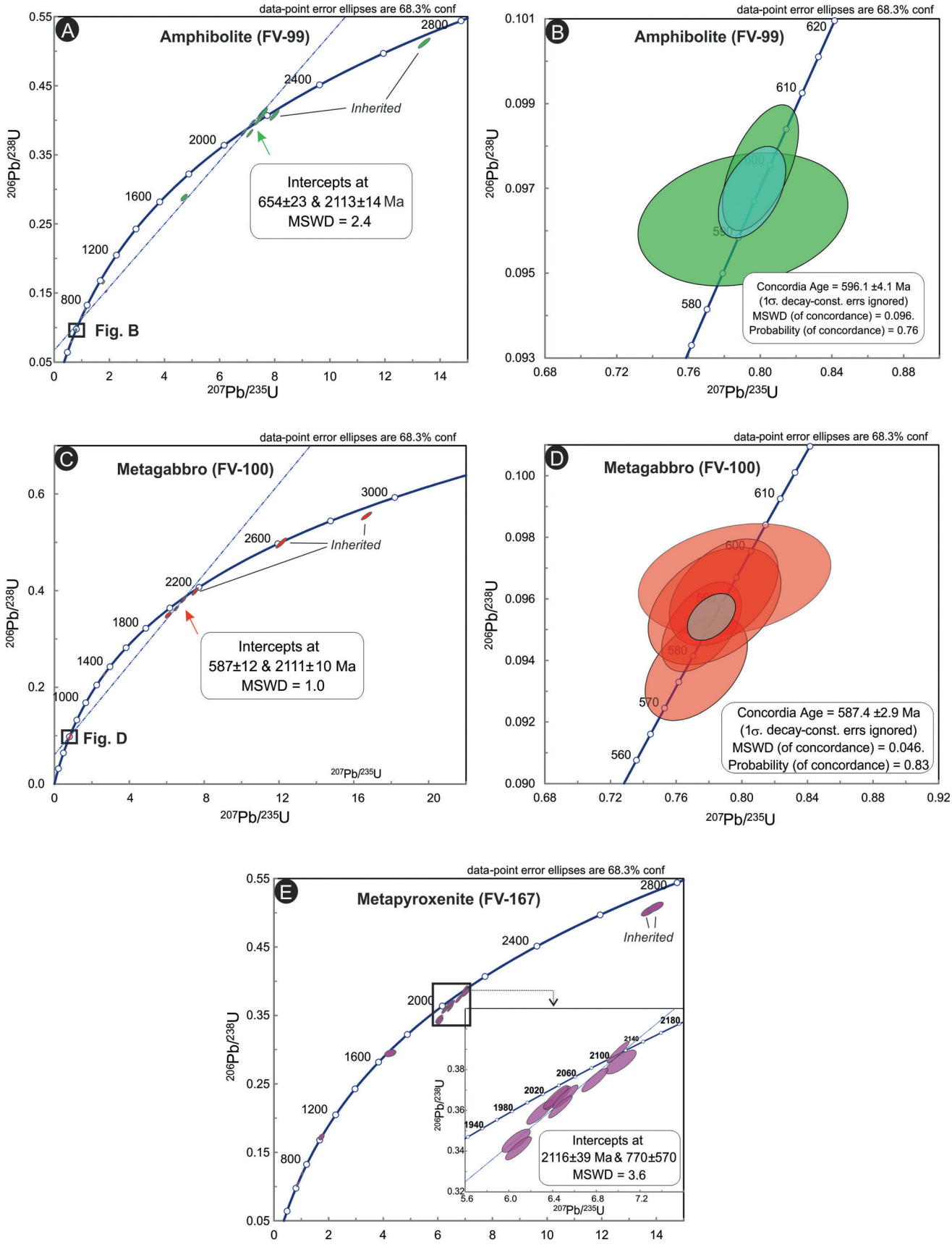


**Figure 11.** Concordia diagrams with 1σ ellipses error for U-Pb SHRIMP zircon analyses from: (A and B) Amphibolite (FV-99 - deformed gabbroic rock) from the Rio Grande metagabbro; (C and D) Rio Grande metagabbro (FV-100); and (E) Metapyroxenite (FV-167) from the Forro layered metaperidotite-metapyroxenites.

### 6.2. Metagabbro sample (FV-100)

The zircon grains showed textural and morphological features that were grouped into two populations. The first group consists of prismatic to pyramidal subhedral grains ranging around 100–200 µm in length, with ratios of 6:1 (grains 1, 2, 5, 6, 7, and 9; Figure 10(B)). They show internal structures characterized by oscillatory zoning and sectoral zoning (grains 1, 2, 5, and 14). These grains also show evidence of post-magmatic recrystallization, characterized by the development of thin and irregular overgrowth rims with high to low luminescence. Moreover, some grains revealed fractures and dark cores (grains 2 and 9). The second population from the metagabbro also shows typical magmatic features with well-defined sectorial and oscillatory zoning (grains 3, 10, 11, 12, and 13; Figure 10(B)). Zircon crystals are subhedral to euhedral, prismatic, 120–150 µm long, with 2:1 to 4:1 ratios, and generally have higher luminescence. These grains exhibit overgrowth rims of variable thickness (~2–30 µm), irregular boundaries, and consistently high luminescence. Grains 3 and 15 showed resorptive features associated with the cores (Figure 10(B)). Three additional zircon grains recovered from this sample show contrasting features. Grain 14 is subhedral, with 200 µm in length and a 2:1 ratio. It displays notably higher luminescence, with oscillatory zoning at the rim and a striped texture in the core. Grain 8 is anhedral, approximately 150 µm in length with a 3:1 ratio, featuring a central faint, ghost zoning, bordered by a less luminescent, irregular, and zoning-free domain. In contrast, grain 4 is subhedral, about 200 µm long with a 2:1 ratio. It consists of a core surrounded by oscillatory zoning with subtle resorption features, and is rimmed by a thin, high-luminescence domain.

The 16 analyses obtained from 15 zircon grains of the metagabbro show low Pb loss, with discordance values of up to 6%. Most data yielded two main age groups, as plotted in Figure 11(C,D). Ten spots fall along a Discordia line that regress to yield an upper intercept age of 2111 ± 10 Ma with an MSWD of 1.0, which is interpreted as the crystallization age of the metagabbro protolith (Figure 11 (C)). Five other analyses, derived exclusively from the second zircon population, yielded a Concordia age of 587 ± 3 Ma (Figure 11(D)), with an MSWD of 0.046. These younger ages are associated with core analyses and tentatively correlated with localized melt-assisted shear zones, melt patch domains, or neosomes (see previous section). Three other analyses (grains 4, 8, and 14) were concordant to slightly discordant at ca. 2184, 2609, and 2964 Ma, respectively, indicating inherited grains. These revealed oscillatory to sectorial zoning and moderate luminescence.

### 6.3. Metapyroxenite sample (FV-167)

The metapyroxenite sample from the Forro-layered metaperidotite-metapyroxenite (FV-167) has zircon grains displaying a range of textures and morphologies, resembling four distinct populations. The main population is characterized by subhedral to euhedral prismatic grains up to 250 µm in length, ratios of approximately 2:1 to 3:1, and well-defined oscillatory zoning (grains 6, 7, 9, 11, 12, and 16; Figure 10(C)). This population usually exhibits more than one thin overgrowth, reaching up to 10 µm, similar to a high-luminescence rim and a low-luminescence rim. The second population is represented by anhedral grains with an oval shape, 150–200 µm in length, and a ratio of approximately 2:1 (grains 3, 4, and 5; Figure 10(C)). These grains show oscillatory, sometimes irregular, and sector zoning. As in the previous population, these grains showed an overgrown rim, mainly with high luminescence. The third population is also anhedral, with rounded edges and lengths of 60–150 µm (grains 8 and 15; Figure 10(C)). They have well-defined xenocrystic cores discontinued from thick overgrown domains (up to 25 µm), which may exhibit a phantom zone. They also have thin overgrowth rims. Finally, the fourth population includes elongated prismatic grains with lengths of 200–300 µm (grains 1 and 2; Figure 10(C)). These grains displayed plane-parallel zoning with weak evidence of homogeneous features.

Fifteen analyses were performed, which presented up to 11% discordance. Ten analyses of the first population of grains were aligned along a Discordia line that regressed to yield an upper intercept age of 2116 ± 39 Ma with MSWD = 3.6 (Figure 11(E)). This date was interpreted as the crystallization age of the metapyroxenite protolith. Two analyses from medium-grey core spots yielded approximately 2800 Ma (grains 3 and 4) and inherited zircon. Additionally, four analyses from three and four populations were dispersed along the Concordia curve, reflecting variable Pb losses. This suggests the onset of a Neoproterozoic overprint, as indicated by two other groups of analyses.

## 7. Sm-Nd isotopic systematics

Supplementary Table S5 presents the Sm-Nd analytical data for seven samples: three from the Rio Grande metagabbro and four from the Forro metaperidotite-metapyroxenite. The $\varepsilon Nd_{(t)}$values were calculated at 2.11 Ga, considering the crystallization age of the protolith.

Amphibolite and metagabbro from the Rio Grande metagabbro have positive (+0.03 to +0.13) $f_{Sm/Nd}$ values, while all samples from the Forro metaperidotite-

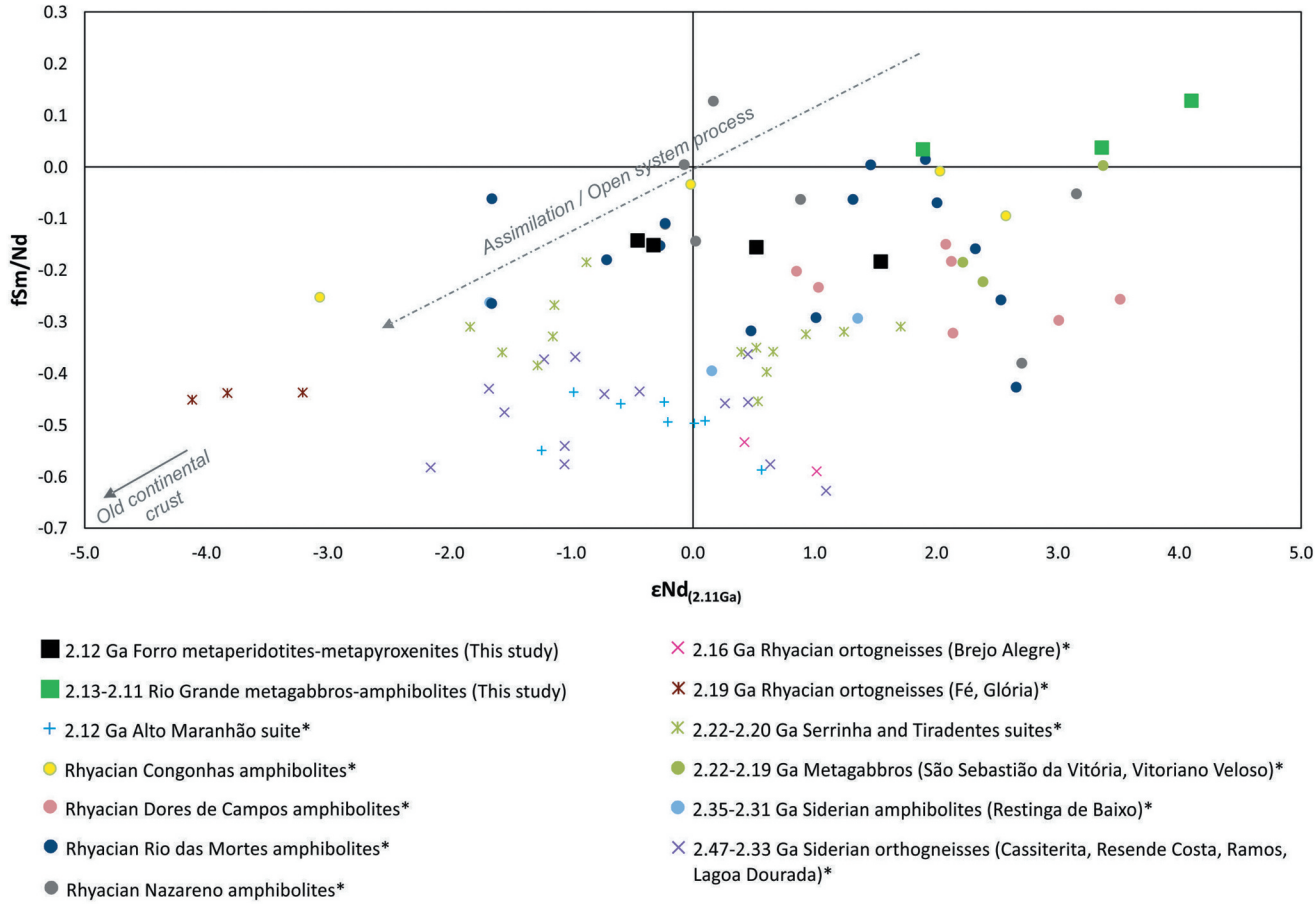


**Figure 12.** εNd(2.11 Ga) versus fSm/Nd diagram for different lithotypes of the main units of the Mineiro belt in the study area and its surroundings. *data compiled from Toledo (2002), Ávila *et al*. (2006, 2010, 2014), Seixas *et al*. (2012, 2013), Teixeira *et al*. (2015), Barbosa *et al*. (2019), and Silva *et al*. (2020).

metapyroxenite have negative (−0.14 to −0.18) $f_{Sm/Nd}$ values (Figure 12). Most samples have positive $\varepsilon Nd_{(t)}$ (+0.52 to +4.10), indicating depleted magma sources, while the slightly negative $\varepsilon Nd_{(t)}$ values (−0.32 and −0.46) of two samples from the Forro metaperidotite-metapyroxenite (CT-190I and CT-190II) point to LREE enrichment. Figure 12 also highlights a trend of contamination/assimilation for these rocks, showing similar behaviour to other mafic rocks within the Mineiro belt.

The two calculated $T_{DM}$ model ages for the Forro metaperidotite-metapyroxenite are similar (2.78–2.72 Ga), indicating a Neoarchean magmatic reservoir.

## 8. Discussion

### 8.1. Timing of the mafic-ultramafic magmatism

The ages of 2111 ± 10 Ma and 2113 ± 14 Ma for the metagabbro and amphibolite of the Rio Grande metagabbro (Figure 11(A,C)), respectively, and the age of 2116 ± 39 Ma for the metapyroxenite from the Forro-layered metaperidotite-metapyroxenite (Figure 11(E)) provide U-Pb SHRIMP reliable crystallization ages for the protoliths, correlating with the Rhyacian evolution in the Mineiro belt (Table 1).

The presence of zircon grains in basic liquids requires processes beyond simple igneous crystallization, such as partial melting of hydrated peridotites (Borisova et al. 2020, 2021) or interaction with crustal-derived fluids and/or crustal recycling (Belousova *et al*. 2015; Bea *et al*. 2018, 2021; Pinheiro *et al*. 2019). At a regional scale, arc magmatism, such as several 2.10–2.13 Ga calk-alkaline suprasubduction-related suites within Mineiro belt (Barbosa *et al*. 2015; Cardoso *et al*. 2019) and the 2.13 Ga Alto Maranhão sanukitoid (Seixas *et al*. 2013), are consistent with the hypothesized mantle refertilization imprinted in the chemical signatures of the samples. Indeed, accretionary orogens involving subduction zones may cause hydrous melting of the overlying mantle wedge by crustal-derived fluids from the slab (e.g. Moreira *et al*. 2020; Lacerda *et al*. 2024). The ages of the Rio Grande (2.14–2.10 Ga) and Brumado (2.12 Ga)

metadiorites from the Ritápolis arc and Gentio metagranitoid (2.10 Ga) point to the genesis involving the subduction of juvenile crust with assimilation of metasedimentary rocks (Cardoso *et al*. 2019; Silva *et al*. 2021).

Chemical imprints of crustal-derived material are characterized by trace element patterns, such as positive Pb and Sr anomalies and the relative enrichment of incompatible lithophile elements (e.g. LREE and LILE) (Figure 9(E,F)), as well as subchondritic $\varepsilon Nd_{(t)}$ values. It is also noteworthy the presence of exogenous Paleoproterozoic and Archaean zircon grains with ages of 2167 ± 7 Ma, 2257 ± 11 Ma, and 2746 ± 8 Ma in the amphibolites; 2184 ± 14 Ma, 2615 ± 11 Ma, and 2964 ± 9 Ma in the metagabbro; and 2811 ± 15 Ma and 2821 ± 16 Ma in the metapyroxenite (Figures 10 and 11A-C).

### 8.2. Igneous processes and signatures

Binary diagrams normalized to immobile elements, including $Al_2O_3$, Ti, Yb, and Zr, for samples of the Rio Grande metagabbro and layered Forro metaperidotite-metapyroxenite allow inferences for the primary geochemical signatures and crystallization and evolutionary pathways of the protoliths (Figure 13(A-F)). Cr and high field strength elements (HFES) showed good correlation when normalized to immobile elements, suggesting that post-magmatic alteration was limited for both bodies.

The precursor rocks of the Rio Grande Metagabbro underwent evolution through plagioclase fractionation (Figure 13(A,B)). In the Forro samples, the compatible behaviour of elements such as Ni and Cr in progressively evolved melts suggests that their protoliths evolved mainly by the fractionation of non-aluminous phases, primarily chromite, olivine, and pyroxene (Figures 9(D,E) and 13C-E). The Rio Grande metagabbro and the Forro-layered metaperidotite-metapyroxenite plot in the transitional zone between the *N*- and E-MORB basalts (Figure 13(F)), without the involvement of garnet in their residues, as evidenced by their enriched flat heavy REE patterns (Figure 9(G)). The normalized trace element patterns show a slightly enriched and flat-designed curve, with enrichments in the order of two to four times their normalized values (Figure 9(F,G)). Indeed, most samples showed positive juvenile $\varepsilon Nd_{(t)}$ (+0.52 to +4.10), which suggests LREE depletion in their mantle sources.

Moreover, the slightly negative $\varepsilon Nd_{(t)}$ values (−0.32 and −0.46) presented by the two Forro samples suggest the involvement of crustal-derived materials. The chemical trend delineated in Figure 13F for the Rio Grande amphibolites and metagabbro also suggests some influence of crustal elements, although to a lesser extent. Exogenous-derived material contaminants were also evidenced by the presence of inherited Archaean grains obtained in both samples from the Forro and Rio Grande plutons, as well as by the enrichment of lithophilic elements such as Sr, Pb, and Rb (see Figure 9(F,G)).

Considering the disturbance of some immobile elements, such as Yb and Nb, there is evidence that the primary chemical signature of these rocks underwent chemical modification after their liquid extraction, without attaining chemical equilibrium prior to the onset of fractionation or differentiation. While further petrological effort is required to determine whether the LILE and LREE enrichments are the result of assimilation, metasomatized mantle sources, or post-magmatic alteration, our data do not avoid the role of metamorphism. From a petrogenetic perspective, the chemical imprints indicate fractional crystallization driven by pristine magmas derived from juvenile enriched sources originating from the Rio Grande metagabbros, while minor crustal contamination may have influenced the evolution and magma fractionation of the Forro-layered rocks. We also noted that some chemical anomalies, such as Rb and LREE enrichment, could be achieved through anatexis, as illustrated in Figure 13(D), allowing lithophile disbalancing. However, due to its limited presence, this chemical interference is considered not pervasive and localized, as attested in the field work, and by the presence of poikilitic mesocumulate crystals and post-cumulus oikocrysts.

### 8.3. Metamorphic overprints and timeline

Figure 14 presents a model for the petrogenetic process of the Rio Grande metagabbro and Forro-layered metaperidotite-metapyroxenite. At least four main metamorphic assemblages demonstrate the metamorphic overprints of these rocks.

The first metamorphic assemblage (M1) is associated with pervasive and static early hydration that occurred immediately after the crystallization of the mafic and ultramafic protoliths at ca. 2.11 Ga. This hydration is enhanced by high thermal gradients and may be related to seafloor-type metamorphism. In the Rio Grande metagabbros, its effects are associated with the recrystallization of Ca-plagioclase into oligoclase (and albite) and epidote aggregates, in addition to the breakdown of primary clinopyroxene into metamorphic pseudomorphs of actinolite (Al Figure 5(F)). This is consistent with typical greenschist facies metamorphism. In the Forro-layered metaperidotite-metapyroxenite, pervasive early serpentinization, with the onset of chlorite and magnetite after primary igneous olivine and pyroxenes, can also be associated with low- to medium-grade metamorphism (Figure 14).

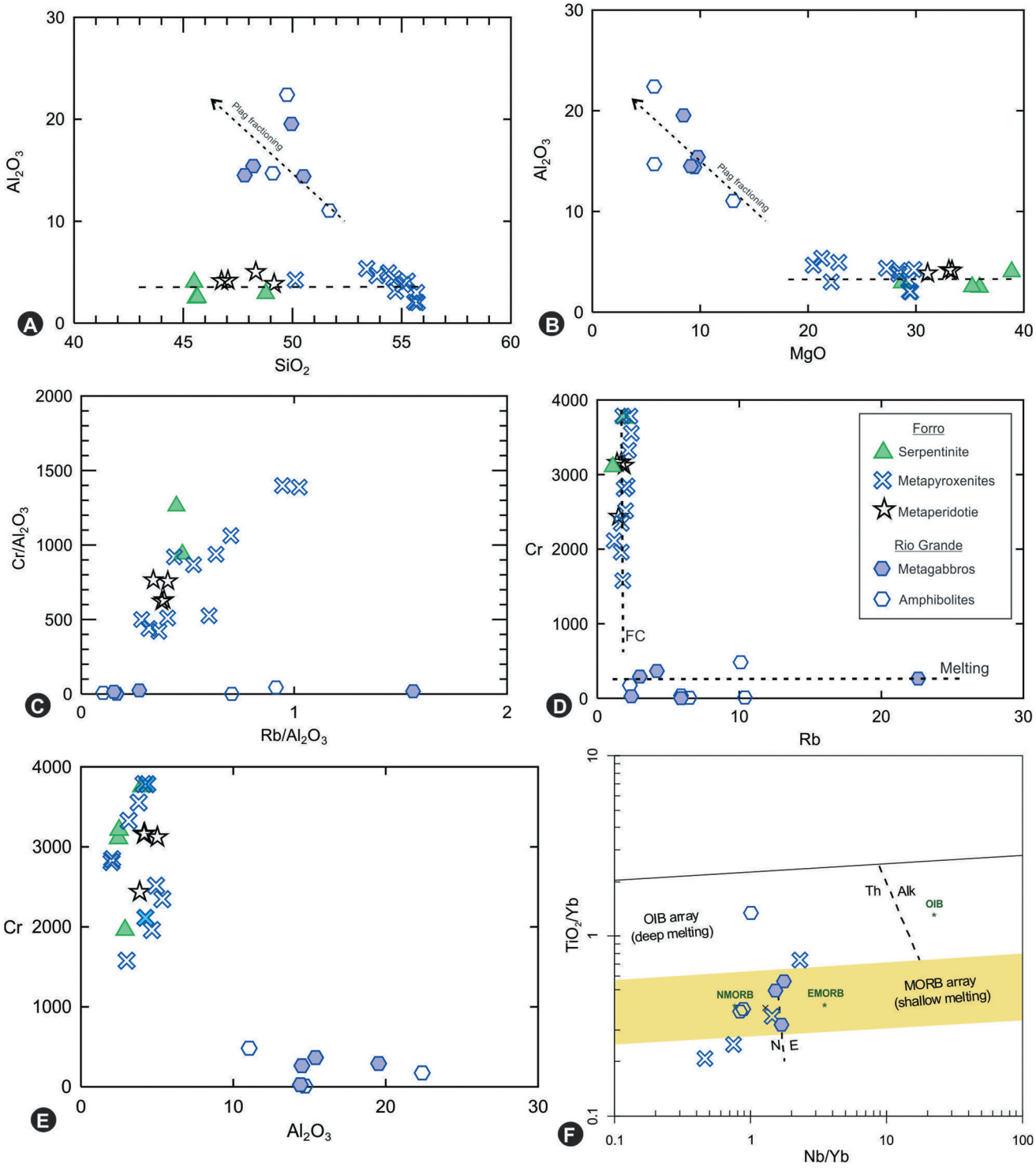


**Figure 13.** Binary diagrams as proxy of petrogenetic processes. (A) Al2O3 (wt%) x SiO2 (wt%). (B) Al2O3 (wt%) x MgO (wt%). (C) Cr (ppm)/Al2O3 (wt%) x Rb (ppm)/Al2O3 (wt%). D) Cr (ppm) ×Rb (ppm); E) Cr (ppm) ×Al2O3 (wt%); F) TiO2/Yb ×Nb/Yb (Pearce 2008).

At the Mineiro belt realm, the M1 event can be related to greenschist facies metamorphism (biotite + albite + epidote + titanite ± chlorite ± muscovite ± sericite ± clinozoisite paragenesis) observed in the nearby 2.14–2.11 Ga Gentio and Macuco de Minas metagranitoides (Silva *et al.* 2021; Neves *et al.* 2023) and the Rio Grande and Brumado metadiorites (Cardoso *et al.* 2019).

The second metamorphic assemblage (M2) is associated with a prograde dynamic recrystallization process. Rocks of the Rio Grande metagabbros are represented

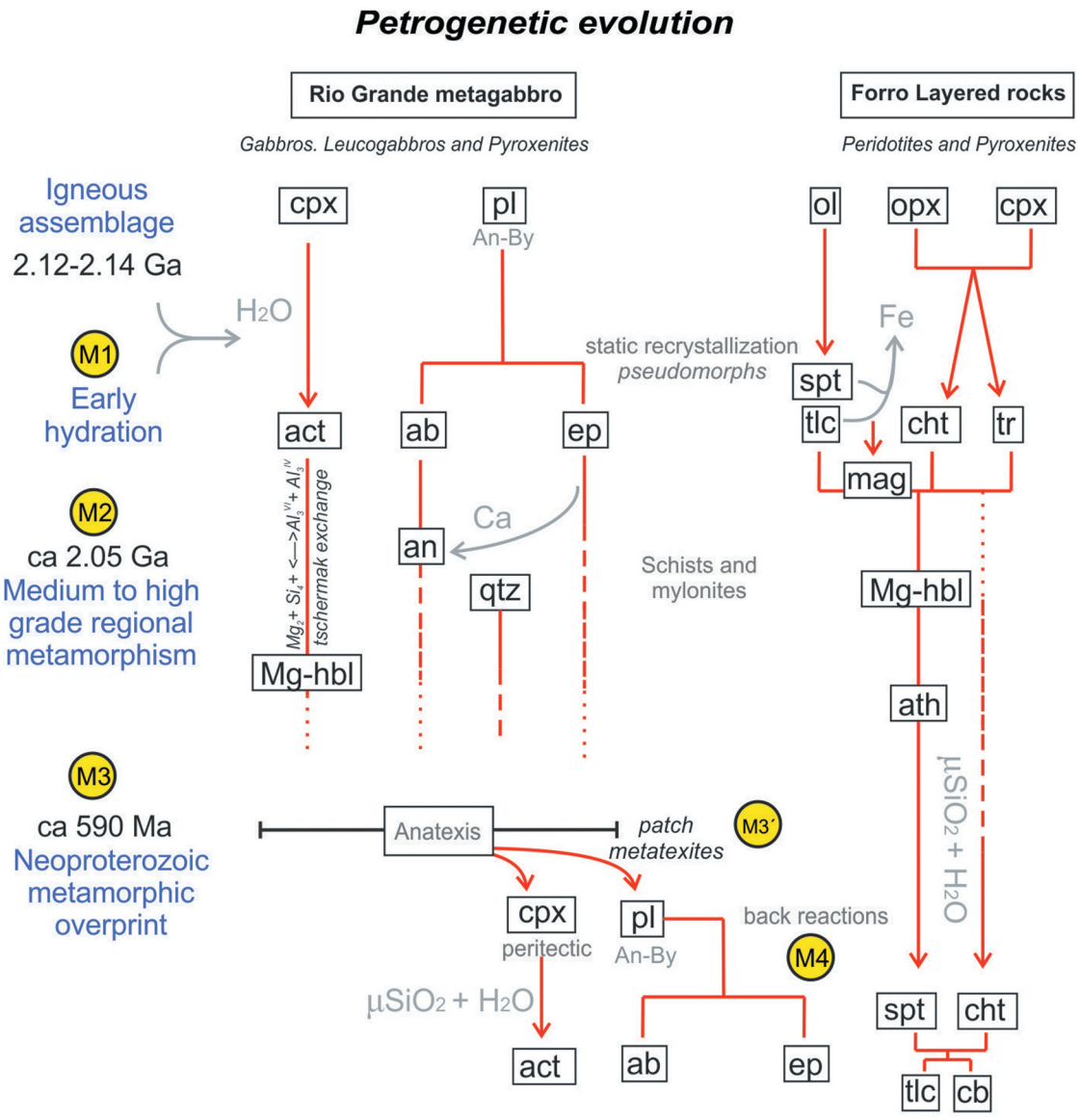


**Figure 14.** Petrogenetic evolution of the Rio Grande metagabbro and Forro layered metaperidotite-metapyroxenites with four metamorphic events, along with their mineral phases and subsequent modifications. Abbreviations: ab: albite; act: actinolite; an: anorthite; ath: anthophyllite; by: bytownite; cb: carbonate; cht: chlorite; cpx: clinopyroxene; ep: epidote; mag: magnetite; Mg-hbl: magnesium-hornblende; ol: olivine; opx: ortopyroxene; pl: plagioclase; qtz: quartz; spt: serpentine; tlc: talc; tr: tremolite.

by: (i) progressive substitution of actinolite to magnesium-hornblende in the metagabbroic rocks (Figure 5(E)); (ii) elongation and stretching of magnesium-hornblende in metagabbroic rocks and nematoblastic-textured amphibolite generations (Figure 5(C,D)); and (iii) recrystallization and re-orientation of plagioclase and epidote grains in metagabbros and amphibolites. This metamorphism reached amphibolite facies, as indicated by the typical assemblage of magnesium-hornblende and plagioclase (oligoclase) in mafic rocks. In the Forro-layered metaperidotite-metapyroxenite, this event is associated with the dynamic recrystallization of serpentine and chlorite aggregates and the onset of tremolite, cummingtonite, and anthophyllite (Figure 14).

The Rio Grande metadiorite, a batholith that outcrops close to the studied amphibolites and metagabbro, has similar metamorphic assemblages of amphibolite facies, exemplified by magnesium-hornblende + actinolite + Na-feldspar (oligoclase or albite) + epidote ± titanite ± zoisite ± clinozoisite ± sericite (Cardoso *et al*. 2019). The M2 metamorphic assemblage is likely associated with a dynamic regional metamorphic event, as the late stage of Paleoproterozoic accretion developed in the Mineiro belt, which occurred between 2.05–1.90 Ga (Cardoso

*et al*. 2019; Teixeira *et al*. 2022; Neves *et al*. 2023; Lacerda *et al*. 2024). A thermo-tectonic event of ca. 2.05 Ga (e.g. orogenic collapse) is widespread along the eastern SFC and reworked margins, preceding its stabilization at 1.90 Ga (Alkmim and Teixeira 2017). The correlative episodes are: (i) the 2.05–1.96 Ga associated to the HT granulite metamorphism from several areas of the Mantiqueira Province (Cutts *et al*. 2020); (ii) the 2.05–1.98 Ga related to the alkaline magmatism (Bruno *et al*. 2020); (iii) the 2.08–2.04 Ma dome and keel structure in the adjacent foreland Quadrilátero Ferrífero domain (Cutts *et al*. 2019); (iv) 2.04–2.0 Ga peraluminous crustal-derived granitoids (Sousa *et al*. 2023; Lacerda *et al*. 2024) and (v) 2.00–1.90 Ga ages of zircon and titanite grains from metagranitoids and rocks of the supracrustal sequences of the Mineiro belt and correlated units (Teixeira et al. 2015, 2022; Moreira *et al*. 2018; Neves *et al*. 2023).

In the internal and marginal domains of the Rio Grande metagabbro, the third metamorphic assemblage (M3), dated at 590 Ma (rims and newly formed single grains), is recorded by amphibolitic mylonites associated with high-strain zones (Figure 3(C)). This metamorphic-deformational event also produced localized anatectic zones in the metagabbroic rocks of the Rio Grande metagabbro. Melt patch domains characterized these zones with irregular neosomes rich in plagioclase (forming plagioclasites), epidote, and peritectic diopside (Figure 6A,B). Although very localized, these domains indicate fluid-assisted incongruent melting of highly hydrated amphibolitic rocks (plagioclase + magnesium-hornblende), mainly associated with rocks bearing M1 and M2 metamorphic assemblages. This reaction may be expressed by magnesium-hornblende = clinopyroxene + melt ($SiO_2$+$H_2O$) and magnesium-hornblende + plagioclase + quartz ± biotite + $H_2O$ = diopside + melt, where the newly formed liquid (neossome) consists of labradorite-andesine + epidote + water (in excess), forming plagioclasites with labradorite cores and andesine rims (Figure 14).

Partial melting of the amphibolitic protolith reached upper amphibolite facies conditions in the presence of externally derived fluid, especially along the shear zones. The crystallization of magmatic-featured younger zircon grains from the melt-patch domains (neossomes) associated with the amphibolites (Figure 10A; grains 4, 5) and metagabbro (Figure 10B; grains 3, 10, 11, 12, 13) of the Rio Grande metagabbro are related to this anatectic system. Notably, the ca. 590 Ma zircon grains represent the best-constrained Ediacaran metamorphic overprint in the southern region of the Mineiro belt. Similarly, the youngest zircon population of the Forro layered metaperidotite-metapyroxenite may be related to the Neoproterozoic overprint, as suggested by the partial Pb loss of the isotopic systems (see Figure 11E).

This Neoproterozoic event is widespread and well documented along the southern domains of the southern SFC and represents the main period of the Western Gondwana assembly in the region. Cabral and Zeh (2015) described younger Neoproterozoic metamorphic ages of approximately 500 Ma for the Sítio Largo amphibolites, which crystallized at 2188 ± 24 Ma in the eastern Quadrilátero Ferrífero region. Furthermore, metamorphic ages of ca. 590 Ma were obtained in metamafic and metaultramafic rocks along the southern and southwestern extension of the reworked margin of the SFC within the southernmost Brasilia orogen (Pinheiro et al. 2019, 2022). This period is correlated with the post-collisional stages in the southern orogenic units and is associated with exhumation, nappe migration, and retrogression at ca. 635–585 Ma (Frugis *et al*. 2018), and fault reactivation and late intrusive magmatism at ca. 605–580 Ma (Janasi *et al*. 2009; Benetti *et al*. 2024). Evidence of this metamorphic influence occurs in the southern portion of the Mineiro belt and is represented by overgrowth rims in zircon grains from both plutonic (Barbosa et al. 2015, 2019) and supracrustal rocks (Teixeira *et al*. 2022) and K-Ar ages (Teixeira *et al*. 1985). The New Ar-Ar ages obtained by Bongiolo *et al*. (2024) demonstrate the action of a Neoproterozoic metamorphic front that reheated the Archaean – Paleoproterozoic basement at the southern edge of the SFC, including the Rio Grande metagabbro, the Forro layered metaperidotite-metapyroxenite, and the other rocks of the Mineiro belt.

The last metamorphic assemblage (M4) was assigned to a late hydration episode under low-grade conditions. In the Rio Grande metagabbro, this is recorded in the neosomes, such as: (i) oligoclase rims on labradorite/andesine, (ii) partial uralitization of peritectic diopside (Figure 5E); and (iii) high reflectance rims on zircon grains (grains 13; Figure 10B). In the Forro-layered metaperidotite-metapyroxenite, the M4 metamorphic assemblage is expressed by late chlorite, serpentine, and talc over amphibole, early serpentine, and magnetite (Figure 14). These mineral assemblages are products of coeval late hydration associated with localized back reactions in metatexite zones and are part of the widespread low-grade metamorphic overprint associated with orogenic collapse.

### 8.4. Mafic-ultramafic rocks of 2.2–2.1 Ga and metassedimentary sequences in the southern SFC

In the Mineiro belt, the interval between 2.19–2.11 Ga includes the crystallization of the studied metamafic and metaultramafic rocks, and the maximum depositional

age of the metasedimentary rocks of the Nazareno metavolcano-sedimentary sequence (Table 1 and Supplementary Table S1). Detrital zircon analysis of quartzite from this sequence shows a unimodal age spectrum with an average young cluster age of 2182 ± 10 Ma, which is considered its maximum depositional age. Metamorphic ages of ca. 2.05–1.90 Ga were obtained from overgrowth rims around igneous zircon cores of ca. 2.09–2.08 Ga (Teixeira *et al*. 2022).

In the northern block of the Mineiro belt (Figure 2), plutonic metamafic and metaultramafic rocks, mainly metagabbros, metapyroxenites, and metaperidotites, are spatially associated with the Rio das Mortes metavolcano-sedimentary sequence. Metabasalts of this sequence have unimodal age spectra with a maximum depositional age of 2126 ± 47 Ma (Moreira *et al*. 2020) and metamorphism dated to 2.05–1.95 Ga (Teixeira *et al*. 2022), similar to those shown for Nazareno and Dores de Campos metavolcano-sedimentary sequences, as presented below.

The Estação Tiradentes metasedimentary sequence shows the predominance of Rhyacian crustal sources. The deposition of this sequence probably occurred after 2088 ± 12 Ma, according to the U-Pb detrital zircon geochronology of diamictite, ferruginous quartzite, and carbonaceous phyllites (Ávila *et al*. 2014). These metasedimentary units are interpreted to have formed in a back-arc setting and are coeval with the calc-alkaline volcanic-subvolcanic rocks of the Tiradentes and Serrinha suites. The Vitoriano Veloso metagabbro outcrops near these sequences show zircon crystallization ages of 2192 ± 12 and 2185 ± 11 Ma and titanite crystallization age of 2175 ± 32 Ma (Vieira 2015). This metagabbro is the youngest metamafic body in the Tiradentes suite. Its age approached the maximum depositional age (2182 ± 10 Ma) reported for the Nazareno metavolcano-sedimentary sequence (Teixeira *et al*. 2022).

Similar metamafic/ultramafic-bearing metasedimentary sequences were found in the northeast and south of the Mineiro belt. In the northeast, a metasedimentary sequence represented by quartzite interbedded with a Mn formation is considered an extension of the metasedimentary rocks of the Rio das Mortes metavolcano-sedimentary sequence (Teixeira *et al*. 2022). This unit yielded a maximum depositional age of 2075 ± 12 Ma (peaks at 2265, 2150 and 2088 Ma; Cabral *et al*. 2019) and indicating that the sedimentation and associated mafic and ultramafic magmatism acted diachronically along these segments. The minimum age of the metasedimentary unit was constrained by intrusive granodiorite with an age of 1860 ± 8 Ma (Cabral *et al*. 2019).

In the southernmost portion of the Brasilia orogen (south of the Mineiro belt), immature intra-oceanic arc metasedimentary rocks of the São Vicente Complex (Figure 1) occur in association with calc-silicate and metamafic-metaultramafic rocks (Westin *et al*. 2016; Pinheiro *et al*. 2019). These metasedimentary rocks have unimodal age spectrum for detrital zircon grains, with peaks at ca. 2.13 and 2.17 Ga (Westin *et al*. 2016). The interbedded metamafic and metaultramafic rocks have zircon crystallization ages between 2.14–2.12 Ga and are associated with penecontemporaneous magmatism of the basin evolution (Pinheiro *et al*. 2019). To the west, the Campos Gerais Complex (Figure 1), a reworked domain of the São Francisco craton, also hosts Rhyacian metaultramafic rocks with continental arc chemical affinity interbedded with metasedimentary sequences (Table 1). In this domain, disrupted chromitite-bearing metaultramafic rocks have a crystallization age of 2132 ± 7 Ma (Pinheiro *et al*. 2022) and are interlayered with clastic sequences with a maximum depositional age of ca. 2080 Ma (Gengo *et al*. 2019).

These data highlight a continuous and dynamic process of basin evolution and mafic-ultramafic magmatism in the Rhyacian, with contemporary accretionary environments, restricted oceans, and intra-arc basin evolution along the southern SFC, in a scenario of introversion assembly of landmasses during this period.

### 8.5. Rhyacian geodynamic evolution

Although the Paleoproterozoic geodynamics *modus operandi* is under debate (Condie and Aster 2009; Condie and Kröner 2013), the arc-related accretion/collision of the Rhyacian crust presented in the Mineiro belt and in the southern SFC is expressive (Ávila et al. 2010, 2014; Heilbron *et al*. 2017; Cardoso *et al*. 2019; Neves *et al*. 2023; Sousa *et al*. 2023).

These plutonic mafic and ultramafic rocks unravel an episode of magmatism involving N to E-MORB signatured basic liquids in an orogenic realm scenario. Similar accretionary orogens reveal metavolcano-sedimentary sequences and plutonic mafic-ultramafic rocks, such as those present in the Rio Grande metagabbro and Forro layered metaperidotite-metapyroxenite.

In the West African craton, the ca. 2.1 Ga Birimian-Eburnean orogen is dominated by arc-related rocks (Labou *et al*. 2020). In this orogen, plutonic mafic and layered ultramafic rocks from different segments are interbedded with metavolcano-sedimentary sequences containing tholeiitic basalts and calc-alkaline rocks. Their chemical analysis and Sm-Nd isotopic data suggest the existence of different mantle sources and settings for these rocks, involving the geodynamic evolution from MORB-signatured crust to the volcanic arc domain (Labou *et al*. 2020). In the Capricornio orogen, the Western Australian craton, plutonic mafic, and ultramafic

rocks alongside metavolcano-sedimentary sequences display distinct affinities and diachronic evolution for at least 40 Ma. In this orogeny, mafic and ultramafic rocks include 2.07 Ga MORB-signatured rocks juxtaposed with 2.03–2.00 rift-related mafic-ultramafic magmatism. The latter is consistent with the passive margin proposed for the northern Yilgarn craton prior to collision with the Pilbara craton between 1965–1950 Ma (Olierook *et al*. 2018; Tucker *et al*. 2023). In the Northern Laurentia cratonic nuclei, mafic-bearing extensional basins were constrained by detrital systems and revealed a broadly extensional regime along the Western Rae Province after 2.1 Ga. This regime developed over a ca. 2.3 Ga juvenile source, with subsequent inversion at ca. 1.95 Ga (Thiessen *et al*. 2024). This Rhyacian geodynamic evolution is coeval with and reflects that observed in the Mineiro belt and its associated accretionary segments in the southern SFC (Heilbron *et al*. 2017 and references therein). It unravels a broad cycle of extensional events, associated with mafic and ultramafic magmatism at ca. 2.1 Ga across many ancestral Columbia landmasses.

Although there is consensus that the São Francisco and Congo blocks assembled at the Rhyacian – Orosirian boundary, there is no unanimity in the distribution of landmasses in the Paleoproterozoic. In the debate over the composition, geometry, and position of the landmasses during the period from 2.1 to about 1.8 Ga, the proposed Columbia (Hou *et al*. 2008; Cederberg *et al*. 2016; Chaves 2021) and the Central African block (D'Agrella-Filho and Cordani 2017) contrast in concept. The São Francisco-Congo paleocontinent (SFCP) is located at the border of Colombia and juxtaposed to the Amazonian craton, which connects South America to Columbia through the Trans-Amazonian orogeny, which is related to the West African landmasses. However, an alternative model suggests that at around 2.0 Ga, the SFCP, along with Kalahari, Borborema, Trans-Sahara, and Rio de la Plata, were assembled in the Central African Block, a diachronic paleocontinent independent of the Columbia supercontinent (D'Agrella-Filho and Cordani 2017).

Moreover, the timing and correlation of this mafic and ultramafic rocks with dike swarms in the southern São Francisco craton (e.g. Mendes *et al*. 2022) suggest a broader mantle-derived basic magmatism across the São Francisco Paleocontinent. This magmatism may not have been restricted to metavolcano-sedimentary basins, but instead may reflect to a major extensional event involving plume activity and supercontinent break-up. A 2.16 Ga Large Igneous Province (LIP) has been linked to widespread basic magmatism, close to a metamorphic event of ca 2.16–2.14 Ga, whithin the Kaapval craton, and broadly coeval with other cratonic landmasses such as Superior, Wyoming and North Atlantic (Gumsley *et al*. 2025). From this perspective, the new Rhyacian data from Rio Grande e Forro rocks, together with those presented in the southern São Francisco craton, may represent a globally time-correlated basic magmatism associated with LIPS.

Although an integrated, comprehensive, and representative dataset of geodynamic modelling, petrology, and palaeomagnetism is needed to advance palaeogeographic reconstructions, the data presented here provide new clues to the geodynamic evolution of the Rhyacian accretionary system from the Nuna-Columbia perspective. This unravels contemporaneous processes of mantle recycling and melting, basin formation, and plutonic mafic and layered mafic-ultramafic magmatism that took place shortly after the magmatic lull period (2.30–2.20 Ga; Spencer *et al*. 2018), and the constitution of the early stages of Columbia assembly in 2.1–1.8 Ga.

## 9. Conclusions

This study provides new petrogenetic, geochronological, and isotopic evidence from Rhyacian metamafic and metaultramafic plutonic rocks in the southern São Francisco Paleocontinent (Mineiro belt), contributing significantly to the understanding of Paleoproterozoic crustal evolution. The U-Pb SHRIMP zircon ages of 2111 ± 10 Ma, 2113 ± 14 Ma, and 2116 ± 39 Ma for the Rio Grande metagabbro and Forro metapyroxenite represent the first well-constrained crystallization ages for these units and correlate with the fifth mafic-ultramafic magmatic event (2.18–2.10 Ga) recorded in the region.

Whole-rock geochemistry and Sm-Nd isotope signatures ($\varepsilon Nd_{(t)} = -0.32$ to $+4.10$; TDM = 2.72–2.78 Ga) indicate that these rocks were derived from a depleted mantle source, variably influenced by crustal components. The inherited Archaean and Paleoproterozoic zircon grains further support assimilation/contamination processes during magma evolution.

A multiphase metamorphic history is documented, starting with an early greenschist-facies hydration (M1), followed by Rhyacian-Orosirian regional amphibolite facies metamorphism (M2), an Ediacaran metamorphic event recorded by the development of amphibolitic mylonites associated with high-strain zones and localized anatexis (M3), and concluding with low-grade retrogression (M4).

Importantly, the identification of Neoproterozoic zircon overgrowths (~590 Ma) in melt-patch domains provides the first evidence of localized anatexis in these rocks, likely related to the Western Gondwana assembly and crustal reworking along the craton margins. These results refine the timing and character of

Paleoproterozoic tectono-magmatic processes in the Mineiro belt and support models involving progressive crustal accretion, reworking, and late Neoproterozoic destabilization of the southern São Francisco craton. The integration of petrological, isotopic, and geochronological data strengthens the role of these mafic-ultramafic bodies as key markers for reconstructing both Columbia and Gondwana supercontinent configurations.

## Acknowledgments

The authors are grateful to the Geological Survey of Brazil (SGB-CPRM) and National Museum (UFRJ) for their support. Grants from the Brazilian National Council of Technological and Scientific Development – CNPq (5092018 - Edital Universal and #310822/2020-3 Research Productivity grants), and Fundação de Amparo à Pesquisa do Estado do Rio de Janeiro (FAPERJ, grant 241925). The Instituto Geoatlântico (grant 405653/2022-0) provided partial funding for this research.

## Disclosure statement

No potential conflict of interest was reported by the author(s).

## Funding

The work was supported by the Instituto Geoatlântico [405653/2022-0]; Fundação de Amparo à Pesquisa do Estado do Rio de Janeiro [241925]; Brazilian National Council of Technological and Scientific Development [310822/2020–3].

## References

Alkmim, F.F., Marshak, S., and Fonseca, M.A., 2001, Assembling West Gondwana in the Neoproterozoic: Clues from the São Francisco craton region: Brazil: Geology, v. 29, no. 4, p. 319–322. doi: 10.1130/0091-7613(2001)029<0319:AWGITN>2.0.CO;2

Alkmim, F.F., and Teixeira, W., 2017, The Paleoproterozoic Mineiro belt and the Quadrilátero Ferrífero. *in* Heilbron, M., Cordani, U., and Alkmim, F. eds. São Francisco Craton. Eastern Brazil, Regional Geology Reviews, Springer International Publishing, pp. 71–94. doi: 10.1007/978-3-319-01715-0_5

Ávila, C.A., Teixeira, W., Bongiolo, E.M., and Dussin, I.A., 2014, The Tiradentes suite and its role in the Rhyacian evolution of the Mineiro belt-são Francisco Craton: Geochemical and UPb geochronological evidences: Precambrian Research, v. 243, p. 221–251. doi: 10.1016/j.precamres.2013.12.028

Ávila, C.A., Teixeira, W., Cordani, U.G., Barrueto, H.R., Pereira, R. M., Martins, V.T.S., and Dunyi, L., 2006, The Glória quartz-monzodiorite isotopic and chemical evidence of arc-related magmatism in the central part of the Paleoproterozoic Mineiro belt. Vol. 78, Minas Gerais State, Brazil, Anais da Academia Brasileira de Ciências, pp. 543–556 p. doi: 10.1590/S0001-37652006000300013

Ávila, C.A., Teixeira, W., Cordani, U.G., Moura, C.A.V., and Pereira, R.M., 2010, Rhyacian (2.23 2.20 Ga) juvenile accretion in the southern São Francisco craton, Brazil: Geochemical and isotopic evidence from the Serrinha magmatic suite, Mineiro belt: Journal of South American Earth Sciences, v. 29, no. 2, p. 464–482. doi: 10.1016/j.jsames.2009.07.009

Barbosa, J.S.F., and Barbosa, R.G., 2017, The Paleoproterozoic Eastern bahia orogenic domain. *in* Heilbron, M., Cordani, U., and Alkmim, F. eds. São Francisco Craton. Eastern Brazil, Regional Geology Reviews, Springer International Publishing, pp. 57–69. doi: 10.1007/978-3-319-01715-0_4

Barbosa, N., Leal, A.M., Debruyne, D., Leal, L.B., Barbosa, N.S., Marinho, M., and Koproski, L.M., 2020, Paleoarchean to Paleoproterozoic crustal evolution in the Guanambi-Correntina block, GCB, north São Francisco craton, Brazil, unravelled by U-Pb geochronology, Nd-Sr isotopes and geochemical constraints: Precambrian Research, v. 340, p. 105–614. doi: 10.1016/j.precamres.2020.105614

Barbosa, N.S., Teixeira, W., Ávila, C.A., Montecinos, P.M., and Bongiolo, E.M., 2015, 2.17–2.10 Ga plutonic episodes in the Mineiro belt, São Francisco craton, Brazil: U-Pb ages, geochemical constraints and tectonics: Precambrian Research, v. 270, p. 204–225. doi: 10.1016/j.precamres.2015.09.010

Barbosa, N., Teixeira, W., Ávila, C.A., Montecinos, P.M., Bongiolo, E.M., and Vasconcelos, F.F., 2019, U-Pb geochronology and coupled Hf-Nd-Sr isotopic-chemical constraints of the Cassiterita orthogneiss (2.47–2.41-Ga) in the Mineiro belt, São Francisco craton: Geodynamic fingerprints beyond the Archean-Paleoproterozoic transition: Precambrian Research, v. 326, p. 399–416. doi: 10.1016/j.precamres.2018.01.017

Bea, F., Montero, P., and Palma, J.F.M., 2018, Experimental evidence for the preservation of U-Pb isotope ratios in mantle-recycled crustal zircon grains: Scientific Reports, v. 8, no. 1, p. 12904. doi: 10.1038/s41598-018-30934-4

Bea, F., Morales, I., Molina, J.F., Montero, P., and Cambeses, A., 2021, Zircon stability grids in crustal partial melts: Implications for zircon inheritance: Contributions to Mineralogy and Petrology, v. 176, no. 18, p. 1–13. doi: 10.1007/s00410-021-01772-x

Belousova, E.A., Jiménez, J.M.G., Graham, I., Griffin, W.L., O'Reilly, S.Y., Pearson, N., and Talavera, C., 2015, The enigma of crustal zircons in upper-mantle rocks: Clues from the tumut ophiolite, southeast Australia: Geology, v. 43, no. 2, p. 119–122. doi: 10.1130/G36231.1

Benetti, B., Campos Neto, M.C., Carosi, R., Luvizotto, G., Iaccarino, S., and Montomoli, C., 2024, In-sequence tectonic evolution of Ediacaran nappes in the southeastern branch of the Brasília orogen (SE Brazil): Constraints from metamorphic iterative thermodynamic modeling and monazite petrochronology: Lithos, v. 464-465, p. 107459. doi: 10.1016/j.lithos.2023.107459

Bongiolo, E.M., Renac, C., Ávila, C.A., Gallet, S., and Neumann, R., 2024, Neoproterozoic tectonothermal overprint on the southern São FranciscoCraton basement. Vol. 412, Brazil, Precambrian Research, p. 107537 doi: 10.1016/j.precamres.2024.107537

Borisova, A.Y., Bindeman, I.N., Toplis, M.J., Zagrtdenov, N.R., Guignard, J., Safonov, O.G., and Fehrenbach, J., 2020, Zircon survival in shallow asthenosphere and deep lithosphere: American Mineralogist, v. 105, no. 11, p. 1662–1671. doi: 10.2138/am-2020-7402

Borisova, A.Y., Zagrtdenov, N.R., Toplis, M.J., Bohrson, W.A., Nédélec, A., Safonov, O.G., Pokrovski, G.S., Ceuleneer, G., Bindeman, I.N., Melnik, O.E., Jochum, K.P., Stoll, B., Weis, U., Bychkov, A.Y., Gurenko, A.A., Shcheka, S., Terehin, A., Polukeev, V.M., Varlamov, D.A., Chariteiro, K., Gouy, S., and Parseval, P., 2021, Hydrated peridotite–basaltic melt interaction, part I: Planetary felsic crust formation at shallow depth: Frontiers in Earth Science, v. 9, p. 73. doi: 10.3389/feart.2021.640464

Bruno, H., Elizeu, V., Heilbron, M., Valeriano, C.M., Strachan, R., Fowler, M., Bersan, S., Moreira, H., Dussin, I., Silva, L.G.E., Tupinamba, M., Almeida, J., Neto, C., and Storey, C., 2020, Neoarchean and Rhyacian TTG-Sanukitoid suites in the southern São Francisco paleocontinent, Brazil: Evidence for diachronous change towards modern tectonics: Geoscience Frontiers, v. 11, no. 5, p. 1763–1787. doi: 10.1016/j.gsf.2020.01.015

Bruno, H., Heilbron, M., Valeriano, C.M., Strachan, R., Fowler, M., Bersan, S., Moreira, H., Motta, R., Almeida, J., Almeida, R., Carvalho, M., and Storey, C., 2021, Evidence for a complex accretionary history preceding the amalgamation of Columbia: The Rhyacian Minas-Bahia orogen, southern São Francisco paleocontinent: Brazil: Gondwana Research, v. 92, p. 149–171. doi: 10.1016/j.gr.2020.12.019

Cabral, A.R., and Zeh, A., 2015, Celebrating the centenary of "the geology of central Minas Gerais, Brazil": An insight from the Sítio Largo amphibolite: The Journal of Geology, v. 123, no. 4, p. 337–354. doi: 10.1086/682047

Cabral, A.R., Zeh, A., Pires, F.R.M., Silva, J.F., Carmo, V.E.F., and Tupinambá, M., 2022, Unconformity-covering pillow lava dated at 2.14 Ga: Challenging the "stable-shelf" Minas supergroup of the Quadrilátero Ferrífero: Minas Gerais, Brazil: Geological Journal, v. 57, no. 5, p. 2046–2057. doi: 10.1002/gj.4397

Cabral, A.R., Zeh, A., Vianna, N.C., Ackerman, L., Pašava, J., Lehman, B., and Chrastný, V., 2019, Molybdenum-isotope signals and cerium anomalies in Palaeoproterozoic manganese ore survive high-grade metamorphism: Scientific Reports, v. 9, no. 1, p. 4570. doi: 10.1038/s41598-019-40998-5

Campos Neto, M.C., and Caby, R., 2000, Terrane accretion and upward extrusion of high-pressure granulites in the Neoproterozoic nappes of southeast Brazil: Petrologic and structural constraints: Tectonics, v. 19, no. 4, p. 669–687. doi: 10.1029/1999TC900065

Cardoso, C.D., Ávila, C.A., Neumann, R., Oliveira, E.P., Valeriano, C.M., and Dussin, I.A., 2019, A Rhyacian continental arc during the evolution of the Mineiro belt, Brazil: Constraints from the Rio Grande and Brumado metadiorites: Lithos, v. 326, p. 246–264. doi: 10.1016/j.lithos.2018.12.025

Carvalho, M., Bruno, H., Bersan, S., Storey, C., Mottram, C., Chapman, G., Fowler, M., Valeriano, C., Lana, C., Neto, C., and Heilbron, M., 2024, Rhyacian-Orosirian transitional arc-collisional magmatism in the Archean piedade microcontinent, southern São Francisco paleocontinent. Vol. 404, Brazil, Precambrian Research, p. 107343 p. doi: 10.1016/j.precamres.2024.107343

Caxito, F.A., Hagemann, S., Dias, T.G., Barrote, V., Dantas, E.L., Chaves, A.O., and Campos, F.C., 2020, A magmatic barcode for the São Francisco craton: Contextual in-situ SHRIMP U-Pb baddeleyite and zircon dating of the lavras, Pará de Minas and Formiga dyke swarms and implications for Columbia and rodinia reconstructions: Lithos, v. 374, p. 105708. doi: 10.1016/j.lithos.2020.105708

Cederberg, J., Söderlund, U., Oliveira, E.P., Ernst, R.E., and Pisarevsky, S.A., 2016, U-Pb baddeleyite dating of the Proterozoic Pará de Minas dyke swarm in the São Francisco craton (Brazil) – implications for tectonic correlation with the Siberian, Congo and north China cratons: GFF-Scandinavian Journal of Earth Sciences, v. 138, no. 1, p. 219–240. doi: 10.1080/11035897.2015.1093543

Chaves, A.O., 2021, Columbia (nuna) supercontinent with external subduction girdle and concentric accretionary, collisional and intracontinental orogens permeated by large igneous provinces and rifts: Precambrian Research, v. 352, p. 106017. doi: 10.1016/j.precamres.2020.106017

Condie, K., 2015, Changing tectonic settings through time: Indiscriminate use of geochemical discriminant diagrams: Precambrian Research, v. 266, p. 587–591. doi: 10.1016/j.precamres.2015.05.004

Condie, K.C., and Aster, R.C., 2009, Zircon age episodicity and growth of continental crust: EOS: Transactions American Geophysical Union, v. 90, no. 41, p. 364. doi: 10.1029/2009EO410003

Condie, K.C., and Kröner, A., 2013, The building blocks of continental crust: Evidence for a major change in the tectonic setting of continental growth at the end of the Archean: Gondwana Research, v. 23, no. 2, p. 394–402. doi: 10.1016/j.gr.2011.09.011

Condie, K.C., Pisarevsky, S.A., Puetz, S.J., Spencer, C.J., Teixeira, W., and Faleiros, F.M., 2022, A reappraisal of the global tectono-magmatic lull at ~ 2.3 Ga: Precambrian Research, v. 376, p. 106690. doi: 10.1016/j.precamres.2022.106690

Cutts, K., Lana, C., Alkmim, F., Farina, F., Moreira, H., and Coelho, V., 2019, Metamorphism and exhumation of basement gneiss domes in the Quadrilátero Ferrífero: Two stage dome-and-keel evolution: Geoscience Frontiers, v. 10, no. 5, p. 1765–1787. doi: 10.1016/j.gsf.2019.02.009

Cutts, K., Lana, C., Moreira, H., Alkmim, F.F., and Peres, G.G., 2020, Zircon U-Pb and Lu-Hf record from high-grade complexes within the mantiqueira Complex: First evidence of juvenile crustal input at 2.4–2.2 Ga and implications for the Palaeoproterozoic evolution of the São Francisco craton: Precambrian Research, v. 338, p. 105567. doi: 10.1016/j.precamres.2019.105567

D'Agrella-Filho, M.S., and Cordani, U.G., 2017, The paleomagnetic record of the São Francisco-Congo craton. *in* Heilbron, M., Cordani, U.G., and Alkmim, F.F. eds. São Francisco Craton. Eastern Brazil, Tectonic Genealogy of a Miniature Continent: Cham, Springer, p. 305–320. doi: 10.1007/978-3-319-01715-0_16

D'Agrella-Filho, M.S., Rapalini, A.E., and Trindade, R.I.F., 2022, Paleomagnetism of the main South American Precambrians Cratons: Brazilian Journal of Geophysics, v. 40, no. 2, p. 1–39. doi: 10.22564/brjg.v40i6.2204

Frugis, G.L., Campos Neto, M., and Lima, R.B., 2018, Eastern Paranapanema and southern São Francisco orogenic margins: Records of enduring Neoproterozoic oceanic convergence and collision in the southern Brasília orogen: Precambrian Research, v. 308, p. 35–57. doi: 10.1016/j.precamres.2018.02.005

Gaucher, C., and Frei, R., 2018, The Archean-Proterozoic boundary and the great oxidation event. *in* Sial, A.N., Gaucher, C.,

Ramkumar, M., and Ferreira, V.P. eds. Chemostratigraphy across Major chronological boundaries. John Wiley & Sons Inc., p. 288. doi: 10.1002/9781119382508.ch3

Gengo, R.M., Moraes, R., and Szabó, G.A.J., 2019, Proveniência sedimentar da unidade Serra do Ibituruna na borda Sul do Cráton do São Francisco: Registros de deposição paleoproterozoica: 4° Simpósio sobre o Cráton do São Fransciso/28° Simpósio de Geologia do Nordeste, SBG in Aracaju-CE. doi: 10.13140/RG.2.2.31793.81761

Green, D.H., and Ringwood, A.E., 1969, The origin of basalt magmas. The Earth's crust: Upper Mantle, p. 489–495. doi: 10.1029/GM013p0489

Gumsley, A., Chamberlain, K., Gumsley, A., de Kock, M., Marciniak-Maliszewska, B., Niezabitowska, D., Soderlundm, U., Bylina, A., and Szlęzak, A., 2025, The identification of a ca. 2165–2163 Ma large igneous province on the Kaapvaal craton in southern Africa with implications for chronostratigraphy, paleogeography and environmental change in the early Paleoproterozoic: Precambrian Research, v. 428, p. 107889. doi: 10.1016/j.precamres.2025.107889

Guo, Q., Strauss, H., Kaufman, A.J., Schröder, S., Gutzmer, J., Wing, B., and Farquhar, J., 2009, Reconstructing Earth's surface oxidation across the Archean-proterozoic transition: Geology, v. 37, no. 5, p. 399–402. doi: 10.1130/G25423A.1

Hawthorne, F.C., Oberti, R., Harlow, G.E., Maresch, W.V., Martin, R.F., Schumacher, J.C., and Welch, M.D., 2012, Nomenclature of the amphibole supergroup: American Mineralogist, v. 97, no. 11–12, p. 2031–2048. doi: 10.2138/am.2012.4276

Heilbron, M., Cordani, U.G., Alkmim, F.F., and Reis, H.L., 2017, Tectonic genealogy of a miniature continent. In Heilbron, M., Cordani, U.G, Alkmim, F. F. Eds. São Francisco Craton, Eastern Brazil, Springer, pp. 321–331. doi: 10.1007/978-3-319-01715-0_17

Hou, G.T., Santosh, M., Qian, X.L., Lister, G.S., and Li, J., 2008, Configuration of the late Paleoproterozoic supercontinent Columbia: Insights from radiating mafic dyke swarms: Gondwana Research, v. 14, no. 3, p. 395–409. doi: 10.1016/j.gr.2008.01.010

Irvine, T.N., and Baragar, W.R.A., 1971, A guide to the chemical classification of the common volcanic rocks: Canadian Journal of Earth Sciences, v. 8, no. 5, p. 523–548. doi: 10.1139/e71-055

Janasi, V.A., Vlach, S.R.F., Campos Neto, M.C., and Ulbrich, H.H. G.J., 2009, Associated A-Type subalkaline and high-K calc-alkaline granites in the Itu granite province, Southeastern Brazil: Petrological and tectonic significance: The Canadian Mineralogist, v. 47, no. 6, p. 1505–1526. doi: 10.3749/canmin.47.6.1505

Labou, I., Benoit, M., Baratoux, L., Grégoire, M., Ndiaye, P.M., Thebaud, N., and Debat, P., 2020, Petrological and geochemical study of Birimian ultramafic rocks within the West African craton: Insights from Mako (Senegal) and loraboué (Burkina Faso) lherzolite/harzburgite/wehrlite associations: Journal of African Earth Sciences, v. 162, p. 103677. doi: 10.1016/j.jafrearsci.2019.103677

Lacerda, S., Guitreau, M., Gonçalves, L., Moreira, H., Gonçalves, C.C., Pinheiro, M.A., Castro, C., and Doucelance, R., 2024, Paleoproterozoic sediment-derived magmas reveal a late orogenic stage in the southern São Francisco craton, Brazil: Evidence from petrogenesis of the 2.0 Ga cupim pluton leucogranites: Lithos, v. 490, p. 107852. doi: 10.1016/j.lithos.2024.107852

Lana, C., Alkmim, F.F., Armstrong, R., Scholz, R., Romano, R., and Nalini, H.A., 2013, The ancestry and magmatic evolution of Archaean TTG rocks of the Quadrilátero Ferrífero province, southeast Brazil: Precambrian Research, v. 231, p. 157–173. doi: 10.1016/j.precamres.2013.03.008

Liebmann, J., Spencer, C.J., Kirkland, C.L.E., Bucholz, C., He, X.F., Santosh, M., and Evans, N.J., 2021, Emergence of continents above sea-level influences sediment melt composition: Terra Nova, v. 33, no. 5, p. 465–474. doi: 10.1111/ter.12531

Magalhães, J.R., Pedrosa-Soares, A., Dussin, I., Müntener, O., Pinheiro, M.A.P., Silva, L.C.D., and Baumgartner, L., 2018, First Lu-Hf, δ 18 O and trace elements in zircon signatures from the Statherian Espinhaço anorogenic province (Eastern Brazil): Geotectonic implications of a silicic large igneous province: Brazilian Journal of Geology, v. 48, no. 4, p. 735–759. doi: 10.1590/2317-4889201820180046

Marimon, R.S., Trouw, R.A., Hawkesworth, C.J., Waterkemper, J., Ribeiro, A., Vinagre, R., and Dantas, E.L., 2023, Challenges of dating metasedimentary successions in collisional orogens: A case study of a Neoproterozoic passive margin in West Gondwana: Gondwana Research, v. 113, p. 1–13. doi: 10.1016/j.gr.2022.10.002

Meert, J.G., and Santosh, M., 2022, The Columbia supercontinent: Retrospective, status, and a statistical assessment of paleomagnetic poles used in reconstructions: Gondwana Research, v. 110, p. 143–164. doi: 10.1016/j.gr.2022.06.014

Mendes, M., Lobato, L.M., Caxito, F., Rosière, C.A., Lana, C., and Silva, R.C.F., 2022, Episodic mafic dike swarms (2.0 and 1.7 Ga) in the QuadriláteroFerrífero province, Brazil: Implications for the refinement of the São Francisco craton magmatic barcode and the north China link: Journal of South American Earth Sciences, v. 120, p. 104049. doi: 10.1016/j.jsames.2022.104049

Moreira, H., Seixas, L., Storey, C., Fowler, M., Lasalle, S., Stevenson, R., and Lana, C., 2018, Evolution of Siderian juvenile crust to Rhyacian high Ba-Sr magmatism in the Mineiro belt, southern São Francisco craton: Geoscience Frontiers, v. 9, no. 4, p. 977–995. doi: 10.1016/j.gsf.2018.01.009

Moreira, H., Storey, C., Fowler, M., Seixas, L., and Dunlop, J., 2020, Petrogenetic processes at the tipping point of plate tectonics: Hf-O isotope ternary modelling of Earth's last TTG to sanukitoid transition: Earth and Planetary Science Letters, v. 551, p. 116558. doi: 10.1016/j.epsl.2020.116558

Morimoto, N., Fabries, J., Ferguson, A.K., Ginzburg, I.V., Ross, M., Seifert, F.A., Zussman, J., Aoki, K., and Gottardi, G., 1988, Nomenclature of pyroxenes: Mineralogical Magazine, v. 52, no. 367, p. 535–550. doi: 10.1180/minmag.1988.052.367.15

Neves, C.V.D.S.A., Ávila, C.A., Bongiolo, E.M., Neumann, R., Teixeira, W., Faulstich, F.R.L., and Valeriano, C.M., 2023, Preserved interactions between acid and intermediate magmas in a 2.15–2.10 Ga Rhyacian continental arc: Insights from petrographic, geochemical, and isotopic data of the macuco de Minas metagranitoid, Mineiro belt: Brazil, Lithos, v. 440-441, p. 107048. doi: 10.1016/j.lithos.2023.107048

Olierook, H.K., Sheppard, S., Johnson, S.P., Occhipinti, S.A., Reddy, S.M., Clark, C., and Erickson, T.M., 2018, Extensional episodes in the Paleoproterozoic Capricorn orogen, Western Australia, revealed by petrogenesis and geochronology of mafic–ultramafic rocks: Precambrian Research, v. 306, p. 22–40. doi: 10.1016/j.precamres.2017.12.015

Oliveira, E.P., McNaughton, N.J., Zincone, S.A., and Talavera, C., 2020, Birthplace of the São Francisco craton, Brazil: Evidence from 3.60 to 3.64 Ga gneisses of the mairi gneiss Complex: Terra Nova, v. 32, no. 4, p. 281–289. doi: 10.1111/ter.12460

Pearce, J.A., 2008, Geochemical fingerprinting of oceanic basalts with applications to ophiolite classification and the search for Archean oceanic crust: Lithos, v. 100, no. 1–4, p. 14–48. doi: 10.1016/j.lithos.2007.06.016

Pearce, J.A., 2014, Immobile element fingerprinting of ophiolites: Elements, v. 10, no. 2, p. 101–108. doi: 10.2113/gselements.10.2.101

Pearce, J.A., and Cann, J.R., 1973, Tectonic setting of basic volcanic rocks determined using trace element analyses: Earth and Planetary Science Letters, v. 19, no. 2, p. 290–300. doi: 10.1016/0012-821X(73)90129-5

Pinheiro, M.A.P., Guice, G.L., and Magalhães, J.R., 2022, Archean–Ediacaran evolution of the Campos Gerais domain—A reworked margin of the São Francisco paleocontinent (SE Brazil): Constraints from metamafic–ultramafic rocks: Geoscience Frontiers, v. 13, no. 5, p. 101201. doi: 10.1016/j.gsf.2021.101201

Pinheiro, M.A.P., Suita, M.T.F., Lesnov, F.P., Tedeschi, M., Silva, L. C., Medvedev, N.S., and Sergeev, S.A., 2019, Timing and petrogenesis of metamafic-ultramafic rocks in the southern Brasília orogen: Insights for a Rhyacian multi-system suprasubduction zone in the São Francisco paleocontinent (SE-Brazil: Precambrian Research, v. 321, p. 328–348. doi: 10.1016/j.precamres.2018.12.006

Profeta, L., Ducea, M., and Chapman, J., 2016, Quantifying crustal thickness over time in magmatic arcs: Scientific Reports, v. 5, no. 1, p. 17786. doi: 10.1038/srep17786

Rogers, J.J., and Santosh, M.J.G.R., 2002, Configuration of Columbia, a mesoproterozoic supercontinent: Gondwana Research, v. 5, no. 1, p. 5–22. doi: 10.1016/S1342-937X(05)70883-2

Seixas, L.A.R., Bardintzeff, J.M., Stevenson, R., and Bonin, B., 2013, Petrology of the high-Mg tonalites and dioritic enclaves of the ca. 2130 Ma Alto maranhão suite: Evidence for a major juvenile crustal addition event during the Rhyacian orogenesis, Mineiro belt, southeast Brazil: Precambrian Research, v. 238, p. 18–41. doi: 10.1016/j.precamres.2013.09.015

Seixas, L.A.R., David, J., and Stevenson, R., 2012, Geochemistry, Nd isotopes and U–Pb geochronology of a 2350 Ma TTG suite, Minas Gerais, Brazil: Implications for the crustal evolution of the southern São Francisco craton: Precambrian Research, v. 196-197, p. 61–80. doi: 10.1016/j.precamres.2011.11.002

Silva, L.C., Pedrosa-Soares, A.C., Armstrong, R., Pinto, C.P., Magalhães, J.T.R., Pinheiro, M.A.P., and Santos, G.G., 2016, Disclosing the Paleoarchean to Ediacaran history of the São Francisco craton basement: The Porteirinha domain, northern araçuaí orogen: Brazil, Journal of South American Earth Sciences, v. 68, p. 50–67. doi: 10.1016/j.jsames.2015.12.002

Silva, M.M., Ávila, C.A., Tavares, F.M., Barbosa, N.S., and Teixeira, W., 2021, Genesis of the Gentio Metagranitoid: Post-collisional high-K plutonism within the Mineiro belt, São Francisco craton, Brazil: Journal of Earth Science, v. 32, no. 6, p. 1374–1396. doi: 10.1007/s12583-021-1469-0

Silva, M.M.D., Ávila, C.A., Barbosa, N.D.S., and Teixeira, W., 2020, Caracterização do Ortognaisse Brejo Alegre e sua inserção no contexto evolutivo do Cinturão Mineiro, Cráton do São Francisco: Anuário do Instituto de Geociências, v. 43, no. 2, p. 363–380. In Portuguese doi: 10.11137/2020_2_363_380

Simon, M.B., Bongiolo, E.M., Ávila, C.A., Teixeira, W., Marimon, R. S., and Oliveira, E.P., 2021, Archean sodic metagranitoids from the southern São Francisco craton: Review, petrogenesis, and tectonic implications: Lithos, v. 398, p. 106246. doi: 10.1016/j.lithos.2021.106246

Sousa, S.S.C.G., Ávila, C.A., Neumann, R., Faulstich, F.R.L., and Scholz, R., 2023, Monazite age and composition from a granite-pegmatite system: A link between pegmatites of the São João del Rei Pegmatitic province and the newly defined high-K Restinga metagranite: Minas Gerais, Brazil, Journal of South American Earth Sciences, v. 123, p. 104232. doi: 10.1016/j.jsames.2023.104232

Spencer, C.J., Murphy, J.B., Kirkland, C.L., Liu, Y., and Mitchell, R. N., 2018, A palaeoproterozoic tectono-magmatic lull as a potential trigger for the supercontinent cycle: Nature Geoscience, v. 11, no. 2, p. 97–101. doi: 10.1038/s41561-017-0051-y

Sun, S.S., and McDonough, W.F., 1989, Chemical and isotopic systematics of oceanic basalts: Geological Society, London, Special Publications, Geological Society, London, Special Publications v. 42, no. 1, p. 313–345. doi: 10.1144/GSL.SP.1989.042.01.19

Teixeira, W., Ávila, C.A., Dussin, I.A., and Bongiolo, E., 2022, U-Pb provenance fingerprints of metavolcanic-sedimentary successions of the Mineiro belt: Proxies for the continuity of plate tectonics through the Paleoproterozoic: Geoscience Frontiers, v. 13, no. 5, p. 101293. doi: 10.1016/j.gsf.2021.101293

Teixeira, W., Ávila, C.A., Dussin, I.A., Neto, A.C., Bongiolo, E.M., Santos, J.O., and Barbosa, N.S., 2015, A juvenile accretion episode: 2.35–2.32 Ga in the Mineiro belt and its role to the Minas accretionary orogeny: Zircon U–Pb–Hf and geochemical evidence: Precambrian Research, v. 256, p. 148–169. doi: 10.1016/j.precamres.2014.11.009

Teixeira, W., Fonseca, A.C., Poupeau, G., Padilha, A.V., Zapparolli, L.H., Kawashita, K., and Khoury, M.C., 1985 , Esboço da evolução geotectônica da parte sul do craton do São Francisco: uma interpretação com base nos dados Rb-Sr, K-Ar, Pb-Pb e traços de fissão. *in* Sociedade Brasileira de Geologia, ed. Anais, Belo Horizonte, Instituto de Geociências, Universidade de São Paulo, In Portuguese), p. 383. Available on https://repositorio.usp.br/directbitstream/109751f8-08e5-49e6-b62d-7ed9e72a1c42/0751290.pdf

Thiessen, E.J., Davies, J.H., Dyck, B., Perrot, M.G., and Martel, E., 2024, Detrital zircon U-Pb+ Hf data supports 2.1 Ga extensional and 2.0 Ga syn-orogenic basin in southwest Rae province during early Nuna assembly: Precambrian Research, v. 410, p. 107455. doi: 10.1016/j.precamres.2024.107455

Toledo, C.L.B., 2002, Evolução geológica das rochas máficas e ultramáficas no Greenstone Belt Barbacena, região de Nazareno, MG, [Ph.D. thesis]unpublished: State University of Campinas, p. 274 (In Portuguese). 10.47749/T/UNICAMP.2002.268008

Trouw, R.A.J., Peternel, R., Ribeiro, A., Heilbron, M., Vinagre, R., Duffles, P., Trouw, C.C., Fontainha, M., and Kussama, H.H., 2013, A new interpretation for the interference zone between the southern Brasília belt and the central Ribeira belt: SE Brazil, Journal of South American Earth Sciences, v. 48, p. 43–57. doi: 10.1016/j.jsames.2013.07.012

Tucker, N.M., Payne, J.L., Kemp, A.I., Kirkland, C.L., Smyth, A., Tunmer, W., Harvey, S., Stinear, M., Machuca, A., Suarez, R.S., and De Waele, B., 2023, A newly discovered 2030–2010 ma magmatic suite records the dawn of proterozoic extension on the southern margin of the yilgarn craton: Precambrian Research, v. 397, p. 107192. doi: 10.1016/j.precamres.2023.107192

Valença, J.G., Silva, M.A., Schimdt, R.S., Trouw, R.A.J., and Noce, C.M., 2000, Transamazonian gabronoritic intrusive rocks from the southernmost São Francisco craton. Brazil, *In*, XXXI International Geological Congress, Rio de Janeiro, 2000, In Portuguese.

Vieira, T.A.T., 2015, Geologia, petrografia, geoquímica e geocronologia do metagabro Vitoriano Veloso e sua relação com o cinturão mineiro. Universidade Federal do Rio de Janeiro – RJ, 80 p, (In Portuguese). Available on: https://minerva.ufrj.br/F/?func=direct&doc_number=000856119&local_base=UFR01.)

Westin, A., Neto, M.C.C., Hawkesworth, C.J., Cawood, P.A., Dhuime, B., and Delavault, H., 2016, A paleoproterozoic intra-arc basin associated with a juvenile source in the southern Brasilia orogen: Application of U–Pb and Hf–Nd isotopic analyses to provenance studies of complex areas: Precambrian Research, v. 76, p. 178–193. doi: 10.1016/j.precamres.2016.02.004

Zhao, G., Sun, M., Wilde, S.A., and Li, S., 2004, A paleo-mesoproterozoic supercontinent: Assembly, growth and breakup: Earth-Science Reviews, v. 67, no. 1–2, p. 91–123. doi: 10.1016/j.earscirev.2004.02.003